

Comprehensive Basis-Set Testing of Extended Symmetry-Adapted Perturbation Theory and Assessment of Mixed-Basis Combinations to Reduce Cost

Montgomery Gray and John M. Herbert*



Cite This: *J. Chem. Theory Comput.* 2022, 18, 2308–2330



Read Online

ACCESS |



Metrics & More

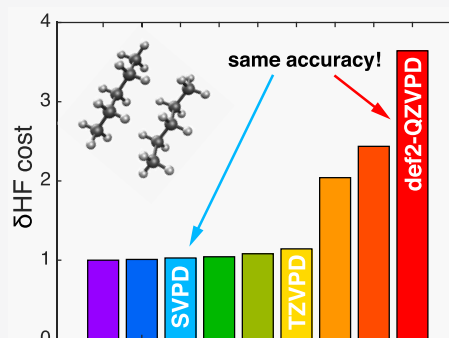


Article Recommendations



Supporting Information

ABSTRACT: Hybrid or “extended” symmetry-adapted perturbation theory (XSAPT) replaces traditional SAPT’s treatment of dispersion with better performing alternatives while at the same time extending two-body (dimer) SAPT to a many-body treatment of polarization using a self-consistent charge embedding procedure. The present work presents a systematic study of how XSAPT interaction energies and energy components converge with respect to the choice of Gaussian basis set. Errors can be reduced in a systematic way using correlation-consistent basis sets, with aug-cc-pVTZ results converged within <0.1 kcal/mol. Similar (if slightly less systematic) behavior is obtained using Karlsruhe basis sets at much lower cost, and we introduce new versions with limited augmentation that are even more efficient. Pople-style basis sets, which are more efficient still, often afford good results if a large number of polarization functions are included. The dispersion models used in XSAPT afford much faster basis-set convergence as compared to the perturbative description of dispersion in conventional SAPT, meaning that “compromise” basis sets (such as jun-cc-pVDZ) are no longer required and benchmark-quality results can be obtained using triple- ζ basis sets. The use of diffuse functions proves to be essential, especially for the description of hydrogen bonds. The “ δ (Hartree–Fock)” correction for high-order induction can be performed in double- ζ basis sets without significant loss of accuracy, leading to a mixed-basis approach that offers 4 \times speedup over the existing (cubic scaling) XSAPT approach.



1. INTRODUCTION

Noncovalent interactions are ubiquitous in nature and drive important chemical processes including crystal packing,^{1–5} protein folding,^{6–10} and host–guest binding in pharmaceuticals,^{11–14} and are important to soft materials of interest in materials science applications.^{15–17} Despite their prevalence, noncovalent forces are often misunderstood by chemists.^{18–20} The framework of symmetry-adapted perturbation theory (SAPT)^{20–26} offers an accurate and systematic *ab initio* approach to noncovalent interaction energies, including an energy decomposition into physically meaningful components: electrostatics, Pauli repulsion, induction, and dispersion.^{27–29} This decomposition is useful for obtaining physical insight that is backed by reliable calculations.^{11,19,20,30–36} The SAPT energy decomposition is inherently more separable than methods based on supramolecular density functional theory (DFT)^{37–39} and can be used to develop physically meaningful force fields.^{1,14,40,41}

The most widely used variant of SAPT, known as SAPT0,^{25,42} combines Hartree–Fock (HF) wave functions for the isolated monomers (as zeroth-order states) with second-order perturbation theory for the intermolecular Coulomb potentials.^{22,25} When used in conjunction with Kohn–Sham (KS) density functionals with correct asymptotic

behavior, intramolecular electron correlation can be incorporated by substituting the KS determinant for the HF one, in a method that we have called SAPT0(KS).^{20,42} The use of asymptotically correct functionals is crucial, and the SAPT0 formalism should not be used with arbitrary density functionals.^{42–44} With that caveat, both traditional SAPT0 and SAPT0(KS) afford semiquantitative results at $O(N^5)$ cost.^{25,42} The accuracy of both methods is limited by the accuracy of the dispersion interactions, which are not quantitative within the “uncoupled” second-order approximation that characterizes SAPT0,^{45–47} and which is similar to second-order Møller–Plesset perturbation theory (MP2).^{48,49}

To obtain quantitative accuracy, second-order dispersion must be replaced by better performing alternatives. This has led to the development of MP2 variants including MP2C⁴⁶ and MP2D,⁴⁷ as well as DFT-SAPT.^{23,24} These methods are much

Received: December 25, 2021

Published: March 15, 2022



more accurate than SAPT0 but retain that method's $O(N^5)$ cost. For MP2C and DFT-SAPT, a density fitting approximation is required in order to obtain fifth-order scaling.^{50,51} This limits DFT-SAPT calculations to dimers with $N \lesssim 100$ atoms.²³ Moreover, the dispersion energy exhibits very slow convergence to the complete basis-set (CBS) limit,⁵² sometimes necessitating the use of explicitly correlated techniques.^{53–55}

The “extended” (X)SAPT approach follows a somewhat similar strategy,²⁰ replacing second-order dispersion with either *ab initio* dispersion potentials (XSAPT + *aiD*)^{48,56–58} or else with a many-body dispersion model (XSAPT + MBD).^{59,60} The latter approach is currently the best-performing variant of XSAPT,^{20,59} and is the primary method used herein. Unlike the aforementioned methods, the cost of XSAPT grows as $O(N^3)$ with respect to the system size (for a fixed basis set),⁴⁸ and has been applied to systems whose monomers are as large as 90–120 atoms.^{20,35,60} It can furthermore be extended to clusters of molecules using a self-consistent charge embedding to capture nonadditive polarization effects.^{58,60–63} For large systems, the monomer-based nature of XSAPT calculations makes this approach more affordable even than supramolecular DFT.^{56,58,59}

Some limited basis-set testing of XSAPT methods has been reported in previous work,^{42,58,59,64} but only for total interaction energies. The present work also examines basis-set convergence for individual energy components, which allows us to evaluate whether earlier tests may have benefited from error cancellation among energy components with different convergence behavior and also to consider mixed-basis combinations in which different energy components are evaluated in different basis sets, taking advantage of the inherent separability of the XSAPT interaction energy. Although the basis-set dependence of traditional SAPT and of DFT-SAPT has been carefully evaluated in previous work,^{25,52} the especially slow convergence of the dispersion energy for those methods means that those tests are not directly relevant to XSAPT. Moreover, previous testing has largely focused on correlation-consistent basis sets, whereas the present work will also test the more affordable Pople and Karlsruhe basis sets.

2. THEORY

The XSAPT formalism^{48,61,62} and the XSAPT + MBD method^{59,60} have been described in previous work, including a recent review.²⁰ For completeness, these methods are briefly summarized below.

2.1. SAPT0(KS). The starting point for XSAPT is second-order SAPT0(KS) for a dimer, for which the total interaction energy (E_{int}) is expressed as^{48,58}

$$E_{\text{int}}^{\text{SAPT0}} = E_{\text{elst}}^{(1)} + E_{\text{exch}}^{(1)} + E_{\text{ind}}^{(2)} + E_{\text{exch-ind}}^{(2)} + E_{\text{disp}}^{(2)} + E_{\text{exch-disp}}^{(2)} + \delta E_{\text{HF}} \quad (1)$$

Superscripts indicate orders in intermolecular perturbation theory but we drop these henceforth, setting $E_{\text{elst}} \equiv E_{\text{elst}}^{(1)}$ (electrostatics) and $E_{\text{exch}} \equiv E_{\text{exch}}^{(1)}$ (exchange or Pauli repulsion). The total induction and dispersion energies are defined, respectively, as

$$E_{\text{ind}} = E_{\text{ind}}^{(2)} + E_{\text{exch-ind}}^{(2)} + \delta E_{\text{HF}} \quad (2)$$

and

$$E_{\text{disp}} = E_{\text{disp}}^{(2)} + E_{\text{exch-disp}}^{(2)} \quad (3)$$

The final term in eq 1, which appears also in eq 2, is a so-called “ δE_{HF} ” correction for higher-order induction effects,^{20,22} defined as

$$\delta E_{\text{HF}} = \Delta E_{\text{int}}^{\text{HF}} - (E_{\text{elst}}^{(1)} + E_{\text{exch}}^{(1)} + E_{\text{ind,resp}}^{(2)} + E_{\text{exch-ind,resp}}^{(2)}) \quad (4)$$

Here, $\Delta E_{\text{int}}^{\text{HF}}$ is the counterpoise-corrected HF interaction energy. The two second-order quantities in eq 4 are response (“resp”) analogues of the second-order terms in eq 2, and these require the solution of coupled-perturbed HF equations.⁶⁵ For SAPT0(KS) calculations, the first- and second-order SAPT terms in eq 4 should be computed at the HF level even if the corresponding terms in eq 1 are computed based on KS orbitals.⁴² Notably, δE_{HF} is the only term in eq 1 that requires self-consistent field (SCF) iterations in a dimer basis set, which becomes a bottleneck for large monomers.

The accuracy of SAPT0(KS) interaction energies depends critically on the use of asymptotically correct exchange-correlation functionals.^{20,42,43} Long-range corrected (LRC) functionals^{66–69} offer a simple means to enforce this constraint, but the range separation parameter must be tuned separately for each monomer in order to obtain correct asymptotics.^{42–44} To this end, we use the LRC- ω PBE functional⁶⁸ combined with the “global density-dependent” (GDD) tuning procedure.^{42,70} As compared to tuning based on the ionization energy criterion,⁴³ GDD-tuning results are essentially identical.⁴²

2.2. XSAPT. The XSAPT approach uses a self-consistent charge embedding procedure based on the variational “explicit polarization” (XPol) formalism.^{60–62,71} In this approach, SCF wave functions for the monomers are computed in the presence of wave function-derived atomic point charges. For this purpose, we use Charge Model 5 (CMS),⁷² whose efficient implementation for XSAPT calculations is described in ref 60. CMS charges are based on the Hirshfeld atomic charge procedure but introduce parameters in an effort to obtain more accurate dipole moments.

The XSAPT + MBD approach starts from the charge-embedded XPol version of SAPT0(KS) but replaces the second-order dispersion energy (eq 3) with a variant of the range-separated and self-consistently screened MBD (or “MBD@rsSCS”) model developed by Tkatchenko and co-workers,^{73,74} although the original approach must be modified at short range for use with SAPT.^{59,60} For a dimer system, this completes the specification of the XSAPT + MBD method.

For a system composed of more than two monomers, the XSAPT interaction energy is²⁰

$$E_{\text{int}}^{\text{XSAPT}} = \sum_A \sum_{B>A} (E_{\text{elst}}^{AB} + E_{\text{exch}}^{AB} + E_{\text{disp}}^{AB} + E_{\text{ind}}^{AB} + \delta E_{\text{HF}}^{AB}) + E_{\text{pol}}^{\text{PW}} + E_{\text{pol}}^{\text{MB}} \quad (5)$$

where the sums run over monomers. The summand in parentheses is the SAPT0(KS) interaction energy for dimer AB, equivalent to eq 1 with MBD replacing second-order dispersion but without charge embedding. The final two terms in eq 5, $E_{\text{pol}}^{\text{PW}} + E_{\text{pol}}^{\text{MB}}$, are the pairwise and many-body polarization energies. The pairwise polarization energy is defined as

$$E_{\text{pol}}^{\text{PW}} = \sum_A \sum_{B>A} [E_{AB}^{\text{XSAPT}}(AB) - E_{AB}^{\text{SAPT}}] \quad (6)$$

where the term in square brackets is the difference between the charge-embedded energy for dimer AB and the SAPT energy computed without charge embedding. The many-body polarization energy is

$$E_{\text{pol}}^{\text{MB}} = \sum_A \sum_{B>A} [E_{AB}^{\text{XSAPT}}(AB \cdots N) - E_{AB}^{\text{XSAPT}}(AB)] \quad (7)$$

where $E_{AB}^{\text{XSAPT}}(AB \cdots N)$ is the energy of dimer AB embedded in an environment of atomic charges corresponding to the entire supersystem $AB \cdots N$, whereas $E_{AB}^{\text{XSAPT}}(AB)$ is the same dimer's energy when embedding charges are included only on monomers A and B . Thus, $E_{AB}^{\text{XSAPT}}(AB)$ is no different from a dimer XSAPT calculation performed on AB in isolation from the rest of the supersystem.

3. COMPUTATIONAL DETAILS

3.1. XSAPT Methods. All calculations were performed using Q-Chem v. 5.⁷⁵ Integral and shell-pair thresholds were set to 10^{-12} a.u., the SCF convergence threshold was set to 10^{-7} Ha, and the SAPT and XSAPT calculations used the “projected” basis set.^{61,62} The latter is an alternative to the dimer basis set that is traditionally used to compute monomer wave functions for SAPT,⁷⁶ but in clusters with more than two monomers this would entail a pairwise SCF cost. In the projected-basis approach, each monomer's SCF wave function is computed in the monomer basis but then a pseudocanonically dimer basis is used for the subsequent pairwise SAPT calculations.^{61,62}

Most calculations reported here are performed at the XSAPT+MBD level of theory,⁵⁹ but some tests will be reported using XSAPT + $aiD3$,^{48,58} where “ $aiD3$ ” denotes the third-generation *ab initio* dispersion potential developed by Lao and Herbert.⁵⁸ The performance of XSAPT + $aiD3$ is marginally better than that of the second-generation version (XSAPT + $aiD2$),⁵⁷ with slightly better coverage of π -stacking in the training set used to parametrize $aiD3$. These methods outperform the first-generation version,⁵⁶ which we do not recommend.^{57,58}

The importance of the δE_{HF} correction, even for SAPT0(KS) calculations that include monomer electron correlation effects, has been noted previously.⁴² Therefore, all XSAPT calculations include the δE_{HF} correction unless explicitly indicated otherwise. As discussed in section 2.1, this correction is computed at the HF level even for SAPT0(KS) and XSAPT calculations.

3.2. Density Functionals. For SAPT0(KS) and XSAPT calculations, the range separation parameter in the LRC- ω PBE functional must be tuned individually for each monomer.^{42–44} We do this at the LRC- ω PBE/def2-TZVP level and then use that value in all subsequent calculations regardless of basis set. (The GDD-tuned values of ω for each of the systems considered in this work can be found in Tables S1–S8 of the Supporting Information.) Previous work has shown that tuned values of ω are sensitive to the fraction of short-range exact exchange, but for a given density functional, these values are rather *insensitive* to the choice of basis set.⁷⁷ The SG-1 quadrature grid⁷⁸ is used for LRC- ω PBE.

3.3. Basis Sets. A standard complement of Pople-style basis sets is tested, ranging in quality up to 6-311++G(3df,2pd).⁷⁹ In modern electronic structure theory these

are often regarded as low-quality basis sets yet they are still widely used, in part because certain quantum chemistry programs (including Q-Chem) have been optimized to take advantage of the use of *sp* functions in Pople basis sets (i.e., *s* and *p* functions with a common exponent). If so, then Pople basis sets are considerably more efficient per unit basis function as compared to other alternatives. Karlsruhe (Ahlrichs) “def2” basis sets are also tested,^{80,81} up to quadruple- ζ quality, as are the correlation-consistent basis sets cc-pVXZ⁸² and aug-cc-pVXZ,⁸³ for $X = D, T, Q,$ and 5 .

In addition to these well-established families of basis sets, we also tested “calendar” versions of the correlation-consistent basis sets,⁸⁴ in which diffuse functions are systematically removed starting from aug-cc-pVXZ. (These basis sets were added to Q-Chem as part of the present work.) The jul-cc-pVXZ basis sets (for $X = D, T,$ or Q) consist of cc-pVXZ for hydrogen and aug-cc-pVXZ for other atoms, meaning that there are no diffuse functions on hydrogen. The jun-cc-pVXZ basis sets additionally remove the diffuse functions with highest angular momentum from each non-hydrogen atom. We note that jun-cc-pVDZ has been suggested as a compromise basis set for SAPT0 calculations,^{25,42} exploiting the slow basis-set convergence of the dispersion energy to limit the intrinsic overestimation of dispersion by second-order perturbation theory. This is a compromise because electrostatics is not generally converged at the double- ζ level,^{42,58} but overall errors in SAPT0 interaction energies are worse in aug-cc-pVDZ and larger basis sets as compared to jun-cc-pVDZ,²⁵ suggesting that it is more important to control the error in second-order dispersion rather than to converge the electrostatics.

We also modified the Karlsruhe basis sets to delete diffuse functions in an analogous manner. As compared to the correlation-consistent basis sets, the Karlsruhe basis sets contain fewer diffuse functions; for example, def2-SVPD contains a diffuse *s* function and a set of diffuse *d* functions for second-row atoms but no diffuse *p* function, and for hydrogen there is a set of diffuse *p* functions but no diffuse *s* function.⁸¹ As a first truncation and in analogy to jul-cc-pVXZ, we delete all of the diffuse functions on hydrogen, forming what is traditionally called a “heavy-augmented” (“ha”) basis set. The basis set consisting of def2-SVP for hydrogen and def2-SVPD for other atoms will therefore be denoted def2-ha-SVP. As a second step, and in analogy to jun-cc-pVXZ, we delete the highest angular momentum set of diffuse functions on each non-hydrogen atom. For second-row atoms, this leaves only minimal augmentation (“ma”) with a diffuse *s* function, so we refer to these basis sets as “def2-ma-”, e.g., def2-ma-SVP. This paradigm is similar in spirit to partially augmented Karlsruhe basis sets tested previously by Zheng et al.,⁸⁵ although the diffuse exponents differ because ref 85 did not start from the standardized Karlsruhe diffuse exponents that were introduced in ref 81. The latter serve as the starting point for our def2-ha and def2-ma basis sets. Exponents and contraction coefficients for these new basis sets are provided in the Supporting Information.

3.4. Data Sets. We will use the S66 data set of dimers⁸⁶ for high-throughput evaluation of a wide variety of basis sets. This database was developed to sample various types of noncovalent interactions, and benchmark interaction energies were reported in ref 86 at the level of coupled-cluster theory with single, double, and perturbative triple excitations [CCSD(T)], extrapolated to the CBS limit. Per the analysis in ref 86, the 66 dimers in this test set are divided into three subsets:

hydrogen-bonded dimers, which are characterized by the condition $|E_{\text{elst}}| \geq 2|E_{\text{disp}}|$; dispersion-dominated dimers, for which $|E_{\text{disp}}| \geq 2|E_{\text{elst}}|$; and dimers of mixed-influence interactions, where neither of these conditions is met. It is useful to group the complexes in this way because the hydrogen-bonded subset (containing 23 dimers involving water, methanol, acetic acid, and other polar monomers) places stringent demands on the basis set as compared to the other S66 systems. The dispersion-bound subset contains 23 dimers involving monomers such as benzene, pyridine, and ethylene.

We will also consider three data sets containing ions:⁸⁷ AHB21, which consists of 21 anion–neutral hydrogen-bonded complexes with ions that include F^- , Cl^- , N_3^- , and SH^- ; CHB6, consisting of cation–molecule complexes of Na^+ , Li^+ , and K^+ with water and benzene; and finally IL16,⁸⁷ which is a set of 16 ion pairs representing constituent molecules or constituent moieties of ionic liquids.⁸⁸ Benchmark interaction energies at the CCSD(T)/CBS level are taken from ref 87 for all three of these ion-containing data sets.

4. RESULTS AND DISCUSSION

4.1. Tests of Traditional SAPT0 Using S66. The basis-set convergence of traditional SAPT methods, including SAPT0 but also higher-order methods, has been reported previously for several small-molecule data sets.²⁵ Nevertheless we include our own SAPT0 convergence tests here, because they establish a baseline to which we can later compare the XSAPT methods, whose alternative descriptions of dispersion lead to accelerated basis-set convergence. Table 1 provides the

Table 1. Error Statistics for SAPT0 Applied to the S66 Data Set

basis set	error (kcal/mol)	
	MAE	max
jun-cc-pVDZ	0.51	1.55
jul-cc-pVDZ	0.64	2.34
aug-cc-pVDZ	0.67	2.49
jun-cc-pVTZ	0.81	3.34
jul-cc-pVTZ	0.93	3.56
aug-cc-pVTZ	1.01	3.70
jun-cc-pVQZ	1.05	3.91
jul-cc-pVQZ	1.09	3.98

mean absolute errors (MAEs) for the S66 database at SAPT0/cal-cc-pVXZ levels of theory, where $X = \text{D}, \text{T}, \text{or } \text{Q}$ and cal = jun, jul, or aug. As previously reported,²⁵ the jun-cc-pVDZ basis set affords the smallest errors, with a MAE of 0.5 kcal/mol and a maximum error of 1.6 kcal/mol. We are unable to complete the SAPT0/aug-cc-pVQZ calculations due to memory limitations on our hardware, but results for other small dimers suggest that MAEs at the SAPT0/aug-cc-pVQZ level are only slightly larger than those at the SAPT0/aug-cc-pVTZ level, by $\lesssim 0.2$ kcal/mol.²⁵

SAPT0 errors increase both with increasing cardinality of the basis set (double-, triple-, or quadruple- ζ) and with increasing augmentation. The reason for this behavior is that the MP2-like second-order approximation that is used in SAPT0 tends to overestimate dispersion significantly, yet dispersion converges very slowly to the CBS limit. More complete basis sets therefore afford increasingly poor dispersion energies, and the use of jun-cc-pVDZ represents something of a “Pauling

point”,⁸⁹ balancing slow convergence against overestimation of the result. It is a remarkably robust compromise in small molecules,^{25,42} although it may fare worse in larger systems.⁴⁸ For example, in the L7 set of large dispersion-bound complexes,⁹⁰ the MAE for SAPT0/jun-cc-pVDZ interaction energies is 4.8 kcal/mol and the maximum error is 10.3 kcal/mol.⁴⁸

SAPT0 dispersion energies for all of the S66 dimers are plotted in Figure 1 using the jun-cc-pVXZ basis sets for $X = \text{D},$

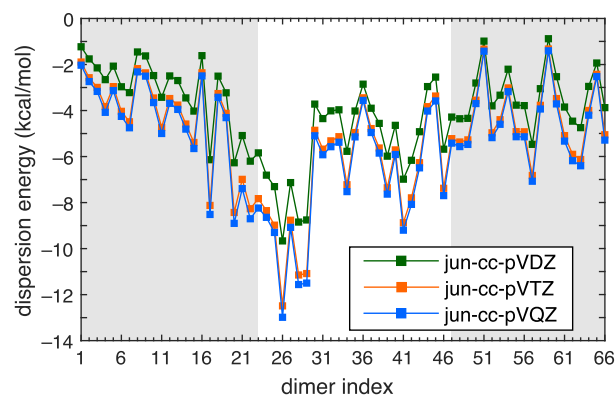


Figure 1. Dispersion energies for the S66 dimers computed at the SAPT0/jun-cc-pVXZ level. Shaded regions delineate the three subsets of S66: hydrogen-bonded dimers (1–23), dispersion-dominated complexes (24–46), and dimers with mixed-influence interactions (47–66).

T, and Q. These data make it clear that the triple- ζ dispersion energies are systematically much larger than double- ζ values, and quadruple- ζ dispersion energies are a bit larger still. As will become clear from the XSAPT data that are presented below, energy components other than dispersion are essentially converged at the triple- ζ level.

4.2. Basis-Set Convergence of XSAPT + MBD. Before embarking on a detailed examination of various basis sets for use with XSAPT + MBD, we first verify the systematic convergence of this method to the basis-set limit using correlation-consistent basis sets aug-cc-pVXZ with $X = \text{D}, \text{T}, \text{Q},$ and 5. To facilitate these large-basis calculations, we use the small-molecule A24 data set,⁹¹ and error statistics for XSAPT + MBD/aug-cc-pVXZ with respect to the CCSD(T)/CBS benchmarks from ref 91 are listed in Table S9. Convergence of the XSAPT + MBD values of E_{int} to within <0.1 kcal/mol is obtained in the triple- ζ basis set, while the $X = \text{Q}$ and $X = 5$ errors are within ~ 0.01 kcal/mol of one another. This already suggests that one of the main goals of the hybrid XSAPT approach has been met, namely, eliminating the very slow convergence of the dispersion energy to the CBS limit.⁵² These calculations also demonstrate that the charge embedding procedure used in XSAPT does not adversely affect or hamper basis-set convergence.

4.3. Survey of Basis Sets for XSAPT + MBD. We next consider the performance of the hybrid XSAPT + MBD method as applied to the S66 dimers. These systems are small, with the largest being pentane dimer, and thereby facilitate high-throughput testing. XSAPT + MBD errors for each of the S66 dimers are plotted in Figure S1 across a wide range of Pople, Karlsruhe, and Dunning basis sets, and these various basis-set families are analyzed separately in the subsections that follow. A statistical survey of the results is

Table 2. Error Statistics for XSAPT + MBD Applied to the S66 Data Set

method	error (kcal/mol)							
	H bonded		dispersion		mixed		all S66	
	MAE	max	MAE	max	MAE	max	MAE	max
def2-SVP	3.71	8.65	2.32	5.33	1.89	2.60	2.67	8.65
def2-ma-SVP	1.86	4.54	1.98	4.47	1.41	2.56	1.86	4.54
def2-ha-SVP	1.14	3.50	1.75	3.74	1.14	2.06	1.35	3.74
def2-SVPD	1.17	3.78	1.65	3.54	1.33	2.30	1.39	3.78
def2-TZVP	0.75	1.67	0.55	1.99	0.82	1.42	0.70	1.99
def2-ma-TZVP	0.19	0.36	0.49	1.78	0.60	1.17	0.42	1.78
def2-ha-TZVP	0.21	0.57	0.50	1.56	0.55	0.99	0.41	1.57
def2-TZVPD	0.17	0.48	0.43	1.57	0.54	0.99	0.37	1.57
def2-QZVP	0.53	2.19	0.36	1.32	0.55	1.17	0.48	2.19
def2-ma-QZVP	0.49	1.94	0.35	1.32	0.49	1.07	0.44	1.40
def2-ha-QZVP	0.40	1.40	0.35	1.08	0.49	1.09	0.41	1.40
def2-QZVPD	0.40	1.36	0.33	1.07	0.49	1.10	0.40	1.36
cc-pVDZ	3.34	8.10	2.42	5.31	1.90	2.68	2.58	8.10
jun-cc-pVDZ	0.98	3.10	0.69	2.09	0.65	1.32	0.78	3.10
jul-cc-pVDZ	0.58	2.64	0.73	2.09	0.62	1.37	0.64	2.64
aug-cc-pVDZ	0.75	2.86	0.77	2.06	0.74	1.52	0.75	2.86
cc-pVTZ	2.18	5.69	1.08	3.15	1.21	1.83	1.50	5.69
jun-cc-pVTZ	0.54	2.51	0.54	1.83	0.53	1.02	0.53	2.51
jul-cc-pVTZ	0.56	2.58	0.52	1.70	0.54	1.03	0.54	2.58
aug-cc-pVTZ	0.60	2.65	0.42	1.60	0.48	1.04	0.50	2.65
cc-pVQZ	0.87	2.84	0.52	2.08	0.78	1.47	0.72	2.84
jun-cc-pVQZ	0.38	1.80	0.32	1.11	0.47	1.00	0.39	1.80
jul-cc-pVQZ	0.44	2.17	0.32	1.17	0.46	0.99	0.40	2.18
aug-cc-pVQZ	0.49	2.41	0.30	1.14	0.44	0.97	0.41	2.41
6-31G(d)	4.74	10.08	3.41	6.74	2.73	3.88	3.67	10.08
6-31+G(d)	2.71	5.71	1.00	2.88	0.99	1.65	1.59	5.71
6-311G(d)	4.23	7.92	2.13	5.12	2.19	2.90	2.88	7.92
6-311G(d,p)	3.54	7.51	2.11	4.91	2.02	2.71	2.58	7.51
6-311+G(d)	2.20	3.51	1.15	3.25	1.31	1.91	1.56	3.51
6-311+G(3df,2pd)	1.04	4.50	0.84	2.47	0.82	1.53	0.90	4.50
6-311++G(d,p)	1.53	3.14	1.02	2.85	1.09	1.55	1.22	3.14
6-311++G(3df,2pd)	0.99	4.43	0.79	2.40	0.77	1.15	0.85	4.43

presented in Table 2, broken down into the three subsets that were described in section 3.4, namely, hydrogen-bonded complexes, dispersion-bound complexes, and dimers with mixed-influence interactions. As with the SAPT0 assessment in section 4.1, error is measured relative to CCSD(T)/CBS benchmarks.⁸⁶

4.3.1. Karlsruhe Basis Sets. Errors for XSAPT + MBD using the Karlsruhe “def2” basis sets are plotted in Figure S1, where the double-, triple-, and quadruple- ζ basis sets have been grouped together by color. Clearly, the double- ζ errors are much larger, exceeding 1 kcal/mol in many cases and typically 1–3 kcal/mol larger than what is obtained in more complete basis sets.

These data also clearly demonstrate the importance of including diffuse functions when calculating interaction energies. This can be seen most clearly from the double- ζ data but is true in triple- and quadruple- ζ basis sets as well, although the magnitude of the effect diminishes with the cardinality of the basis set. For the double- ζ basis sets, errors increase in a consistent way as the diffuse orbitals are trimmed, going from def2-SVPD (with a full complement of diffuse functions) to the “heavy-augmented” def2-ha-SVP basis set, to the “minimally-augmented” def2-ma-SVP basis, and finally to def2-SVP that contains no diffuse functions at all. The importance of diffuse basis functions is most significant in

the hydrogen-bonded subset, where induction effects are important and where the aforementioned truncations of def2-SVPD increase the MAE from 1.2 (def2-SVPD) to 3.7 kcal/mol (def2-SVP), with an increase in the maximum error from 3.8 (def2-SVPD) to 8.7 kcal/mol (def2-SVP). Removal of the diffuse functions has a much smaller effect in systems that are dominated by dispersion.

Removal of the diffuse functions also has a smaller effect at the triple- and quadruple- ζ levels. Whereas in the double- ζ case the use of diffuse functions is absolutely essential to obtain even semiquantitative results, at the triple- or quadruple- ζ level it appears that minimal augmentation is sufficient. We conclude that diffuse functions added to double- ζ basis sets are partially compensating for the overall incompleteness of the monomer basis set, which becomes much less of an issue at the triple- ζ level. We will carefully document the importance of diffuse functions throughout this work, because in our experience many quantum chemistry users are extremely reluctant to include these functions, presumably for reasons of cost.

Examining the error statistics for the Karlsruhe basis sets in Table 2, it appears that absolute errors converge at the triple- ζ level. The differences between triple- and quadruple- ζ interaction energies are uniformly smaller than 1 kcal/mol, and on average these differences are no more than 0.2–0.3

kcal/mol. The largest differences (approaching 1 kcal/mol) are for systems with very strong hydrogen bonds, such as acetic acid dimer, and in those cases the quadruple- ζ errors are actually larger than the triple- ζ errors, by about 0.2 kcal/mol on average, although the maximum errors increase by about 1 kcal/mol. In view of the smooth convergence of XSAPT + MBD interaction energies for the A24 data set when aug-cc-pVXZ basis sets are used (see Table S9), we attribute this slight discrepancy to an artifact of the Karlsruhe basis sets rather than to a deficiency of the XSAPT + MBD method. The Karlsruhe basis sets were originally designed for SCF calculations and not for CBS extrapolation. If systematic convergence to ~ 0.1 kcal/mol is required then Dunning basis sets can be used, albeit at greater cost. Those results are discussed next.

4.3.2. Dunning Basis Sets. Errors for correlation-consistent basis sets and “calendar” variants thereof are provided in Figure S1 with statistics compiled in Table 2. As seen for the smaller molecules in the A24 data set (Table S9), the differences between aug-cc-pVTZ and aug-cc-pVQZ are $\lesssim 0.1$ kcal/mol, and aug-cc-pVSZ results for the A24 dimers suggest that the aug-cc-pVQZ energies are converged.

As with the Karlsruhe basis sets, we find that some augmentation with diffuse functions is necessary to obtain high-quality results for hydrogen-bonded systems despite the fact that all of the monomers in S66 are charge neutral; nevertheless, full augmentation (i.e., the conventional aug-cc-pVXZ) is not necessary to reach convergence. In the absence of any diffuse functions at all, the cc-pVTZ basis set affords unacceptably large errors (up to 5.7 kcal/mol), specifically for the hydrogen-bonded complexes. These errors are substantially reduced by minimal augmentation, e.g., jun-cc-pVDZ or jun-cc-pVTZ, although some of the errors for hydrogen-bonded complexes remain larger than 1 kcal/mol even at the aug-cc-pVTZ level, where the average error is 0.5 kcal/mol but there are outliers up to 2.6 kcal/mol for hydrogen-bonded complexes. In terms of the diffuse functions that are required, the use of jun-cc-pVXZ (for X = D, T, or Q) affords very similar results to aug-cc-pVXZ, indicating that the full complement of diffuse functions is not required even for hydrogen-bonded complexes. This is a useful observation because jun-cc-pVXZ is significantly more scalable to large systems as compared to aug-cc-pVXZ due to the deleterious effects of diffuse functions on integral screening.

The takeaway from this analysis is that the accuracy obtained from these very large basis sets is somewhat more systematic but largely comparable to what is achievable using the somewhat more modest Karlsruhe basis sets. Unlike the case of SAPT0, once the slow convergence of the dispersion energy is taken out of the picture it is no longer the case that jun-cc-pVDZ affords the best results, and the accuracy is improved substantially in triple- ζ basis sets. The data provide no compelling reason to push to quadruple- ζ basis sets, however.

4.3.3. Pople Basis Sets. XSAPT + MBD absolute errors using Pople basis sets are shown in Figure S1, color coded across the visible spectrum based on the size of the basis set, with warmer colors (toward red) indicating larger basis sets. Errors are generally larger as compared to Karlsruhe or Dunning basis sets, although 6-311++G(d,p) and 6-311++G(3df,2dp) perform reasonable well, with MAEs of 1.2 and 0.8 kcal/mol, respectively, although the maximum errors (3.1 and 4.4 kcal/mol, respectively) are larger than those obtained using triple- ζ basis sets of the Karlsruhe or Dunning variety.

Diffuse functions on hydrogen make very little difference, even for hydrogen-bonded systems, and 6-311+G(3df,2dp) affords results that are nearly indistinguishable from 6-311++G(3df,2dp).

These “(3df,2dp)” basis sets were originally developed for MP2 calculations⁹ and provide relatively good performance for the hydrogen-bonded subset of S66, where large induction effects amplify the importance of polarization functions. For the other S66 dimers, however, the performance of these basis sets is nearly identical with that of several other Pople basis sets, notably 6-31+G(d). A set of diffuse functions is necessary even for the dispersion-bound complexes, but otherwise, the double- ζ basis sets perform just as well as the triple- ζ ones for the dispersion-bound and mixed-influence dimers. Polarization functions matter little for dispersion-bound systems and affect the MAEs for that subset by $\lesssim 0.2$ kcal/mol.

Overall, even the best of the Pople basis sets afford larger errors than what is readily achieved with either Karlsruhe or Dunning basis sets, but Pople basis sets can be competitive alternatives of only slightly lower quality, provided that both diffuse and polarization functions are present. The use of composite *sp* shells makes Pople basis sets more efficient per unit basis function as compared to other types of basis sets, assuming that one is using a quantum chemistry program that is written to exploit this. As such, 6-311+G(d,p) and 6-311+G(3df,2dp) may have a place in the pantheon of SAPT methods for large systems.

4.3.4. Summary. Several of the best-performing basis sets from each of the categories discussed above are compared in Figure 2. (Analogous plots for additional basis sets can be

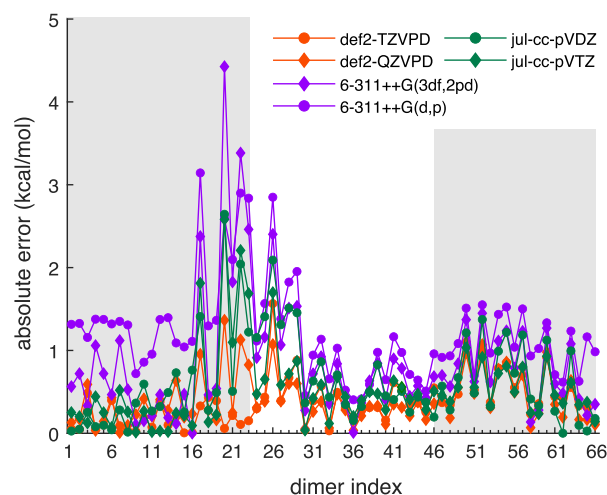


Figure 2. Absolute errors in XSAPT + MBD total interaction energies for the S66 dimers using some of the best-performing basis sets. The index along the horizontal axis refers to the ordering of the S66 dimers in ref 86, and the three regions delineated by shading indicate the hydrogen-bonded subset (dimers 1–23), the dispersion-dominated subset (24–46), and the subset of mixed-influence dimers (47–66). Errors are defined with respect to the CCSD(T)/CBS benchmarks from ref 86. See Figure S1 for additional basis sets.

found in Figure S1.) It is clear that even the best-performing Pople basis sets are outperformed by both Dunning and Karlsruhe basis sets. All of the largest discrepancies are found among the hydrogen-bonded subset of S66; hence, the problem is likely the inadequate description of induction energies, which is confirmed by subsequent analyses presented

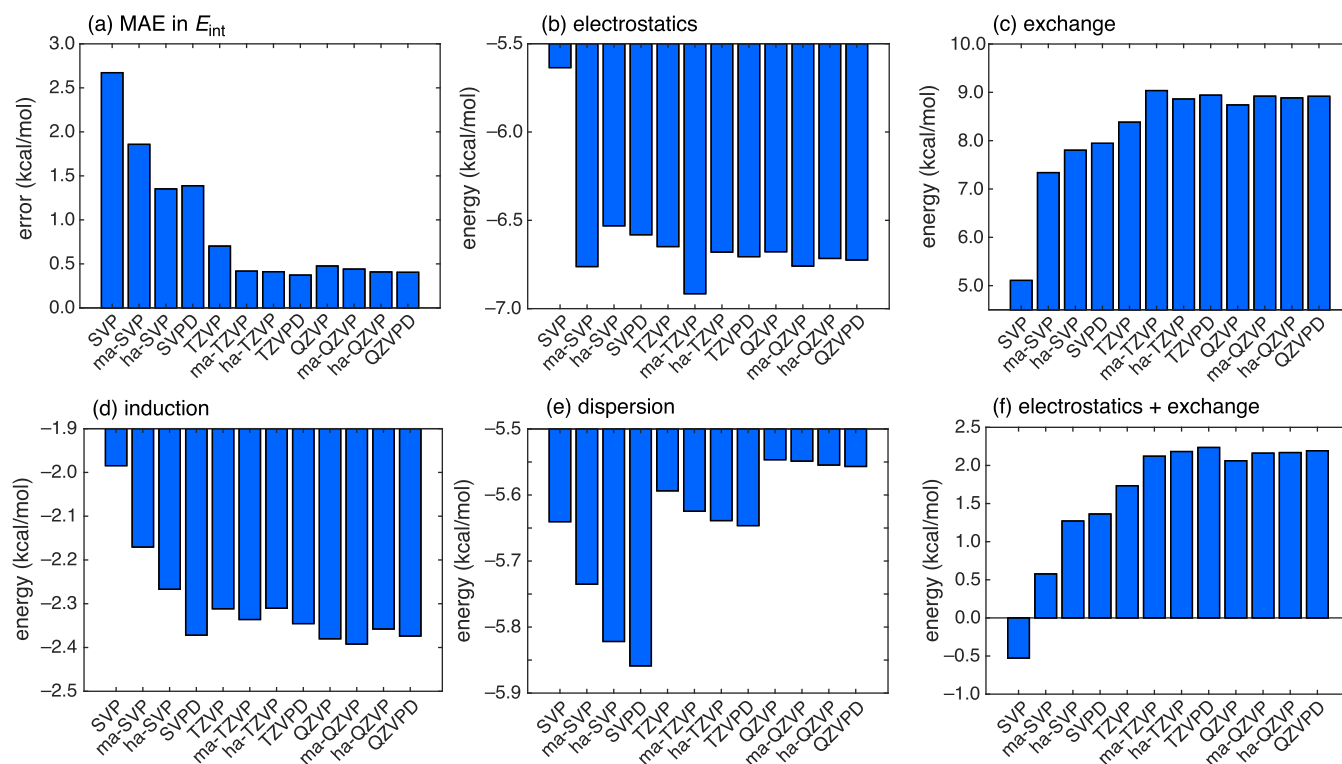


Figure 3. (a) MAEs in E_{int} along with S66-averaged values of (b) E_{elst} , (c) E_{exch} , (d) E_{ind} , (e) E_{disp} , and (f) $E_{\text{elst}} + E_{\text{exch}}$, each computed at the XSAPT + MBD level in various Karlsruhe basis sets. For brevity, “def2” is omitted from the basis-set names.

below. In contrast, the best of the Dunning and Karlsruhe basis sets are nearly identical in their performance, with MAEs < 0.5 kcal/mol. The Karlsruhe basis sets achieve this level of accuracy with fewer basis functions and will therefore be the focus of much of the rest of this work.

4.4. Energy Component Analysis. It is clear from the results in section 4.3 that the largest variations among basis sets occur for hydrogen-bonded complexes, suggesting that the induction energy is more sensitive to the choice of basis set as compared to other energy components. To investigate this further, we next examine how individual energy components converge with respect to basis set. We do this first for the S66 systems that were examined above (in section 4.4.1) and then for the S22 data set⁹² (section 4.4.3). For the latter, high-level SAPT benchmarks are available,⁹³ so we can examine not just convergence but also errors in each energy component.

4.4.1. Averaged Components for S66. Individual energy components for the S66 systems are plotted in Figure S2, where the calculations were performed at the XSAPT + MBD level in each of the six best-performing basis sets that were identified in section 4.3. These data will not be discussed in detail because the variations between basis sets are mostly quite small. This does demonstrate that the basis sets that we previously identified as the best-performing ones achieve this status not through any kind of error cancellation but rather because they offer a converged (or nearly converged) description of each energy component.

In an attempt to distill the S66 data into a form that can be used for quick side-by-side comparison of different basis sets, we will instead examine average values of E_{elst} , E_{exch} , E_{ind} , and E_{disp} across the entire S66 data set. These averages are not physically meaningful because they do not exemplify any one system; nevertheless, inspection of how the average changes

from one basis set to the next provides a simple means to gauge convergence as a function of basis set. This analysis will underscore the fact that not all of the energy components converge in the same way and that some components place different demands on the basis set than others.

As explained in section 3.3, we have tested not only the traditional augmented Karlsruhe basis sets (def2-SVPD, etc.) but also heavy-augmented versions (def2-ha-SVP, etc.) in which diffuse functions are removed from the hydrogen atoms, and minimally augmented versions (def2-ma-SVP, etc.) that further remove the diffuse functions having the highest angular momentum on the other atoms. Finally, the def2-SVP, def2-TZVP, and def2-QZVP basis sets contain no diffuse functions whatsoever.

Figure 3 presents the basis-set dependence of the errors in total interaction energies along with S66-averaged values of each energy component: E_{elst} , E_{exch} , E_{ind} , and E_{disp} . The average dispersion energies are considered in Figure 3e, and in view of the results presented in section 4.4, it is not surprising that all of the basis sets examined afford values within 0.3 kcal/mol of the def2-QZVPD result. As such, we will not consider the dispersion energies in any more detail.

Considering the electrostatic energies (Figure 3b), the def2-QZVPD basis set affords an S66-averaged value $\langle E_{\text{elst}} \rangle = -6.7$ kcal/mol, and all of the basis sets except def2-SVP come within ± 0.2 kcal/mol of this value, including the rather compact def2-ma-SVP basis set. In contrast, when the cardinality of the basis set is increased to the triple- or quadruple- ζ level, augmentation does not appear to be necessary in order to obtain a converged result for electrostatics; the def2-TZVP and def2-QZVP values of $\langle E_{\text{elst}} \rangle$ are both within 0.05 kcal/mol of the def2-QZVPD value.

S66-averaged exchange energies are given in Figure 3c, and these prove to be more sensitive to the choice of basis set. The def2-SVP basis is clearly inadequate and differs by about 4 kcal/mol (or 44%) from the def2-QZVPD value of $\langle E_{\text{exch}} \rangle$. This should be contrasted with the behavior of $\langle E_{\text{elst}} \rangle$, where the entire collection of Karlsruhe basis sets spans a range of less than 1.5 kcal/mol. Also in contrast to the electrostatics case, for exchange it does not seem to be possible to obtain a converged result simply by adding diffuse functions to a double- ζ basis set. However, a triple- ζ basis (with or without diffuse functions) does appear to be adequate: the def2-TZVP result differs by just 0.6 kcal/mol (8%) from the def2-QZVPD result, and the def2-TZVPD value differs by just 0.1 kcal/mol (1%). What is similar to the case of electrostatics and perhaps surprising is that triple- and quadruple- ζ calculations of the exchange energy do not appear to benefit at all from diffuse basis functions. This is reflected in the overall error statistics in the interaction energies (Figure 3a).

The quantity $E_{\text{elst}} + E_{\text{exch}}$ is often grouped together as “electrostatics plus finite size”,^{36,64} or equivalently as the electrostatic interaction between antisymmetrized monomer wave functions.³⁴ This is convenient because the sum of these two energy components is often more comparable in magnitude to the remaining energy components (E_{ind} and E_{disp}), whereas electrostatics and exchange individually are often much larger in magnitude but opposite in sign, at least where equilibrium geometries are concerned. The average basis-set dependence of $E_{\text{elst}} + E_{\text{exch}}$ is presented in Figure 3f. On the ~ 1 kcal/mol energy scale, it is clear that a triple- ζ basis set is required to obtain converged results but that only minimal augmentation is needed in that case. The def2-SVP result is qualitatively wrong, but even with a full complement of diffuse functions (i.e., def2-SVPD), the results are clearly inferior to def2-TZVP. Convergence is reached at def2-ma-TZVP.

Average induction energies are presented in Figure 3d. Whereas the def2-SVP value of E_{ind} is underestimated by 2.0 kcal/mol (17%), all of the other values lie within 0.2 kcal/mol (8%) of the def2-QZVPD result. Remarkably, a double- ζ basis set with diffuse functions affords values of E_{ind} that are close to the def2-QZVPD values, and in a triple- ζ basis set the diffuse functions are not needed to obtain a value that is negligibly different from the def2-QZVPD value. This may suggest a tractable computational scheme for large systems in which the induction energy is computed in a smaller basis set as compared to electrostatics or exchange. First, however, we will more rigorously examine this conclusion in section 4.6 using ion–water clusters that exhibit much larger induction energies as compared to the S66 systems.

Looking back at the errors in total interaction energies (Figure 3a), we see that none of the double- ζ basis sets achieves an MAE below 1 kcal/mol. On the basis of the analysis presented in this section, we ascribe this failure primarily to an inadequate description of E_{elst} and E_{exch} since E_{ind} and E_{disp} are reasonably well described in double- ζ basis sets so long as diffuse functions are included. The def2-TZVP basis set affords a mean accuracy < 1 kcal/mol despite the absence of diffuse functions, without benefiting significantly from error cancellation. With minimal augmentation (def2-ma-TZVP), the MAE drops below 0.5 kcal/mol and the average deviation in each energy component is $< 3\%$ of the def2-QZVPD value. The def2-ma-TZVP basis set therefore appears

to afford converged XSAPT + MBD results, at least for the S66 dimers.

4.4.2. Distance Dependence. To examine the distance dependence of the interaction energies, we selected two complexes from the S66 $\times 8$ data set,⁸⁶ namely, acetic acid dimer and the parallel-displaced benzene dimer. S66 $\times 8$ contains CCSD(T)/CBS interaction energies at various intermolecular separations ranging from $R = 0.9R_e$ to $R = 2.0R_e$ in multiples of the equilibrium separation R_e , and XSAPT + MBD errors for acetic acid dimer are plotted in Figure 4 as a function of intermolecular separation. (See Figure

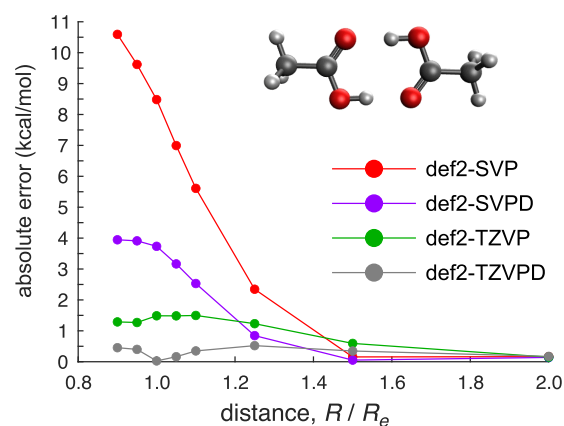


Figure 4. Absolute error in the XSAPT + MBD interaction energy, as compared to the CCSD(T)/CBS benchmark, for acetic acid dimer as a function of intermolecular separation. Geometries and benchmark values of E_{int} come from the S66 $\times 8$ data set.

S3 for the analogous benzene dimer data.) Using double- ζ basis sets, the errors for both systems are observed to increase dramatically at short range ($R \lesssim 1.25R_e$), consistent with the severe underestimation of exchange repulsion in double- ζ basis sets that was noted above. For the triple- ζ basis sets, however, errors for $R < R_e$ are not significantly larger than those obtained at the equilibrium geometry, although the data do highlight the importance of diffuse basis functions (comparing def2-TZVP to def2-TZVPD) for the description of hydrogen bonds. For $R \geq 1.5R_e$, the errors using both double- and triple- ζ basis sets have converged to within < 1 kcal/mol for acetic acid dimer. For benzene dimer, these basis sets are indistinguishable for $R \geq 1.5R_e$, consistent with the rapid basis-set convergence of the dispersion energy.

4.4.3. Benchmark Components for S22. In this section, we examine the basis-set behavior of individual energy components for the S22 data set,⁹² comparing XSAPT + MBD (in various basis sets) to energy components computed at the SAPT2+(3)/aug-cc-pVTZ level.⁹³ The latter approach affords an overall MAE of 0.5 kcal/mol for the S22 interaction energies with respect to CCSD(T)/CBS benchmarks, which can be separated into a MAE of 0.8 kcal/mol for the electrostatically dominated subset versus 0.2 kcal/mol for the remaining systems.²⁵ We therefore take the SAPT2+(3)/aug-cc-pVTZ results to be benchmarks for each individual energy component.

Figure 5 plots the error in each energy component for each S22 dimer in several basis sets. We restrict our attention to the best-performing Pople and Karlsruhe basis sets that were identified in section 4.3, omitting the Dunning basis sets since the S66 results suggest that comparable, high-quality XSAPT +

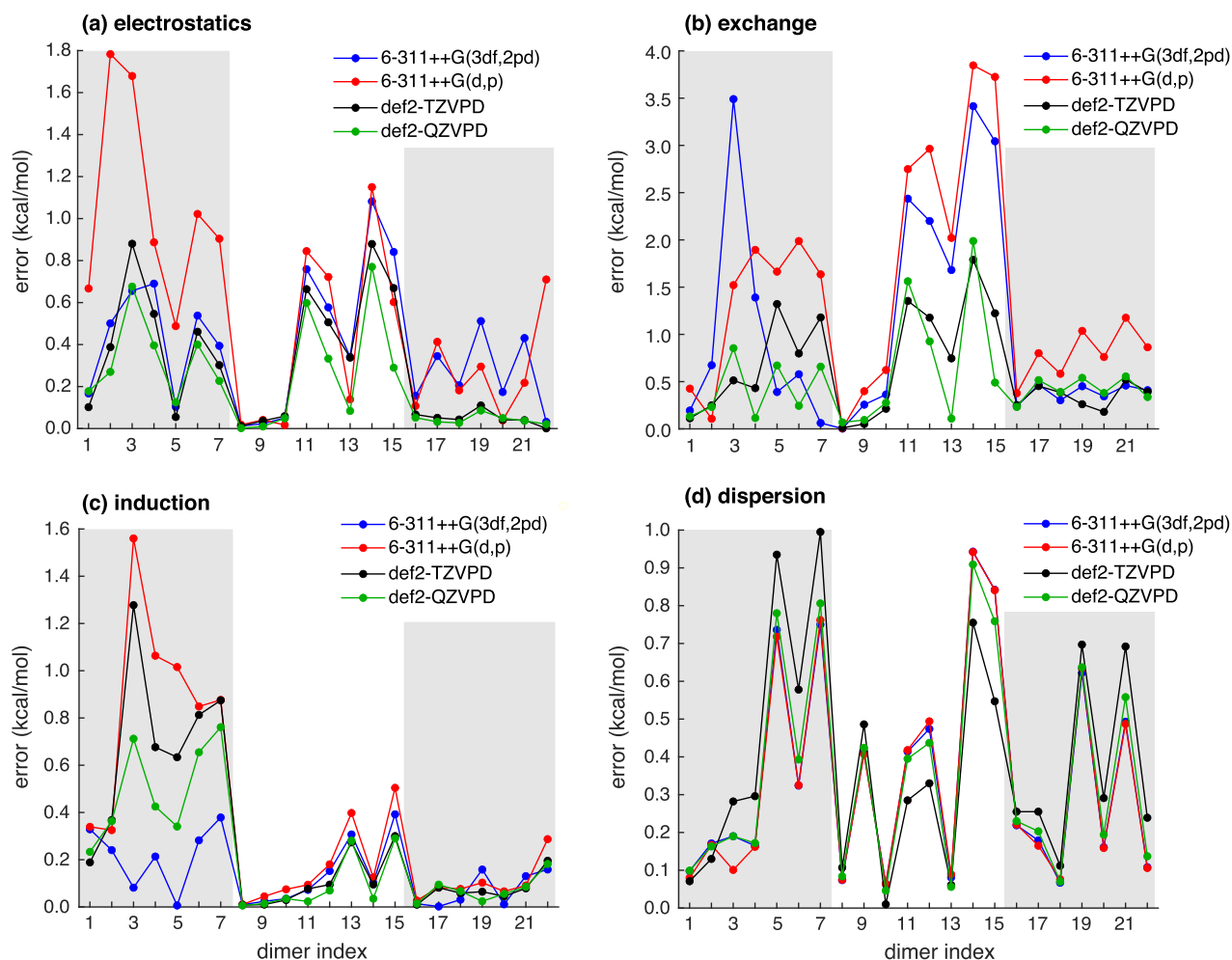


Figure 5. Absolute errors in energy components for the S22 dimers, computed at the XSAPT + MBD level in the basis sets that are shown and compared to benchmark energy components computed at the SAPT2+(3)/aug-cc-pVTZ level. Shaded regions delineate the electrostatics-dominated dimers (1–7), dispersion-dominated dimers (8–15), and dimers with mixed-influence interactions (16–22). Note that the energy scale is different in each panel.

MBD energetics can be obtained more efficiently using def2-TZVPD and def2-QZVPD. Examining the electrostatic energies in Figure 5a, we notice that 6-311++G(d,p) exhibits errors $\gtrsim 1.0$ kcal/mol for several of the electrostatically dominated systems (dimers 1–7 in Figure 5) with the largest errors for $(\text{H}_2\text{O})_2$ and $(\text{HCO}_2\text{H})_2$ (dimers 2 and 3, respectively). With addition of polarization functions to obtain 6-311++G(3df,2pd), the electrostatic errors for these same complexes are comparable to those obtained using def2-TZVPD or def2-QZVPD. More surprising is that 6-311++G(3df,2pd) outperforms both Karlsruhe basis sets for the induction energies (Figure 5c). Errors in the exchange energies (Figure 5b) are significantly larger for both Pople basis sets than they are for either Karlsruhe basis set. This is especially true for the formic acid dimer (system 3) and for the four π -stacked dimers (systems 11, 12, 13, 14, and 15 representing, respectively, the dimers of benzene, pyrazine, and uracil and the heterodimers indole...benzene and adenine...thymine). Consistent with the analysis in section 4.4.1, the dispersion energy is rather insensitive to the choice of basis set.

Overall, the picture that emerges from these data are that the somewhat larger errors for hydrogen-bonded complexes that were documented for S66 dimers when the 6-311++G(3df,2pd) basis set is used (MAE of 1.0 kcal/mol and

maximum error of 4.4 kcal/mol, whereas the maximum error for def2-TZVPD is 0.5 kcal/mol) result primarily from an inadequate description of exchange rather than electrostatics or induction. The def2-TZVPD basis set offers reasonably consistent performance for each energy component, with errors that are $\lesssim 1.5$ kcal/mol in each.

4.5. Benchmarks Containing Ions. Systems containing ions tend to exhibit much larger interaction energies as compared to cases where the monomers are charge neutral, and this may place different demands on basis sets. We next consider results for the IL16, AHB21, and CHB6 data sets of ion-containing dimers that were described in section 3.4.⁸⁷ Despite some promising preliminary results using XSAPT + MBD to describe ion–molecule interactions,^{36,60,64} we identified other cases where the performance of the MBD model is erratic for ion-containing systems, perhaps due to issues relating to the nonuniqueness of the Hirshfeld partition in such cases, for which iterative schemes have been suggested^{94–96} and implemented with supramolecular DFT-based versions of the MBD model.^{97–99} (Alternative means of obtaining polarizabilities for use in the MBD model have also been shown to be superior to the original MBD@rsSCS approach.¹⁰⁰) In view of these difficulties, we consider that a proper MBD model for ion-containing systems is still under

Table 3. Error Statistics for XSAPT + *aiD3* Applied to Ion-Containing Data Sets^a

basis set	error (kcal/mol)					
	IL16		AHB21		CHB6	
	MAE	max	MAE	max	MAE	max
jun-cc-pVDZ	2.53 (2.3%)	5.75	3.12 (12.9%)	13.12	1.46 (5.0%)	3.11
jul-cc-pVDZ	1.09 (1.0%)	3.18	2.26 (11.0%)	7.69	2.05 (6.3%)	6.19
aug-cc-pVDZ	1.29 (1.2%)	3.54	1.86 (8.0%)	7.36	2.01 (6.2%)	6.50
jun-cc-pVTZ	0.80 (0.8%)	3.07	1.76 (8.4%)	6.44	2.09 (6.4%)	7.21
jul-cc-pVTZ	1.28 (1.2%)	3.46	1.48 (7.0%)	5.69	2.32 (7.1%)	7.57
aug-cc-pVTZ	1.71 (1.6%)	3.83	1.27 (5.8%)	5.70	2.09 (6.3%)	7.06
jun-cc-pVQZ	1.17 (1.1%)	2.79	1.43 (6.9%)	6.18	1.53 (4.8%)	4.40
jul-cc-pVQZ	1.44 (1.3%)	3.38	1.28 (6.2%)	7.80	1.69 (5.1%)	5.53
aug-cc-pVQZ	1.72 (1.6%)	3.69	1.23 (5.5%)	8.18	1.31 (3.8%)	4.74
def2-ma-SVP	3.11 (2.8%)	5.60	3.70 (16.7%)	11.93	1.83 (6.7%)	3.43
def2-ha-SVP	1.03 (1.0%)	2.60	2.86 (13.5%)	8.38	1.20 (4.3%)	2.56
def2-SVPD	1.23 (1.1%)	2.60	2.49 (11.3%)	8.14	1.52 (5.3%)	2.89
def2-ma-TZVP	1.95 (1.8%)	3.78	2.61 (11.2%)	8.57	1.74 (5.9%)	3.86
def2-ha-TZVP	1.24 (1.1%)	2.30	2.73 (12.3%)	8.24	1.28 (4.1%)	3.68
def2-TZVPD	1.08 (1.0%)	2.29	2.54 (11.1%)	8.36	1.26 (4.0%)	3.65
def2-TZVPPD	0.85 (0.8%)	2.16	1.89 (8.9%)	6.09	1.63 (5.0%)	5.78
def2-ma-QZVP	1.44 (1.3%)	3.44	1.39 (7.0%)	3.20	1.76 (5.3%)	3.20
def2-ha-QZVP	1.23 (1.1%)	2.60	1.51 (7.6%)	3.03	1.43 (4.4%)	4.97
def2-QZVPD	1.24 (1.1%)	2.63	1.46 (7.3%)	3.06	1.20 (3.8%)	3.96
def2-QZVPPD	1.24 (1.1%)	2.63	1.46 (7.3%)	3.06	1.21 (3.8%)	3.96
6-311+G(3df,2pd)	8.33 (8.1%)	18.12	1.76 (8.2%)	8.28	2.98 (8.8%)	10.38
6-311++G(3df,2pd)	8.32 (8.1%)	18.09	1.74 (8.1%)	8.09	2.95 (8.7%)	10.26

^aRelative to CCSD(T)/CBS benchmarks from ref 87. Boldface values indicate the best-performing basis sets.

development. For the present purposes, however, we have already demonstrated that the MBD dispersion energy converges rapidly with basis set, because the density converges rapidly, and do not expect this to be different for an ionic MBD model. We will therefore focus on the other energy components in this section, using the XSAPT + *aiD3* method.⁵⁸ In this approach, E_{disp} is modeled using atom-atom C_6/R^6 and C_8/R^8 potentials and does not depend on the density at all, but the other three energy components are computed in the same manner as in XSAPT + MBD, so the conclusions should be transferable.

XSAPT + *aiD3* error statistics for the IL16, AHB21, and CHB6 data sets are compiled in Table 3. For these calculations, monomer SCF wave functions are computed using the monomer basis set in order to preclude any charge delocalization at the SCF level, although the dimer basis is still used for the δE_{HF} calculations because $\Delta E_{\text{int}}^{\text{HF}}$ in eq 4 needs to be counterpoise corrected. Because the IL16 and AHB21 data sets contain anions, only basis sets containing diffuse functions are considered in these tests.

The first column of Table 3 gives the error statistics for the IL16 database of cation–anion pairs, and these errors are also plotted in Figure 6a for the Dunning and Karlsruhe basis sets. Notably, 6-311++G(3df,2pd) proves to be on par with the other triple- ζ basis sets in systems containing either cations (CHBH) or anions (AHB21), with a MAE of 2.95 or 1.74 kcal/mol, respectively. However, when cations and anions are in the system (IL16) the MAE increases substantially, to 8.32 kcal/mol

Perhaps serendipitously, the best-performing basis set for IL16 is jun-cc-pVTZ with a MAE of 0.8 kcal/mol, although the def2-ha-SVP and def2-TZVPPD basis sets afford comparable MAEs, and def2-TZVPPD affords a smaller maximum error.

(The def2-TZVPD basis set is nearly as good as def2-TZVPPD.) In contrast to the behavior for S66, here we see no systematic improvement in accuracy for larger basis sets, although the errors do not get significantly larger. For example, the XSAPT + *aiD3*/aug-cc-pVXZ methods with X = D, T, and Q afford MAEs of 1.3, 1.7, and 1.7 kcal/mol, respectively, and maximum errors of 3.5, 3.8, and 3.7 kcal/mol. Similar trends hold for the Karlsruhe sequence of basis sets (def2-SVPD, def2-TZVPD, and def2-QZVPD), although the errors are slightly but systematically smaller in the Karlsruhe basis sets as compared to the Dunning basis sets. As noted in a previous SAPT study,⁸⁷ the most challenging systems in these ion-containing data sets require a “ δ MP2” correction for higher-order induction (and not just a δ HF correction), in order to achieve < 1 kcal/mol accuracy with respect to CCSD(T)/CBS benchmarks. As such, errors of 1.7 (MAE) or 3.7 kcal/mol (maximum) obtained at the XSAPT + *aiD3*/aug-cc-pVQZ level likely reflect the inherent accuracy of this particular XSAPT-based method as applied to these very challenging ion-pair systems. Some error cancellation is then responsible for the somewhat better performance of the smaller basis sets mentioned above.

Figure 6b–d shows the energy components (excluding dispersion) for the IL16 data set. The electrostatics term (Figure 6b) is especially flat, with variations of no more than 1 kcal/mol across a wide range of Karlsruhe and Dunning basis sets. Excluding the double- ζ basis sets, because we know that E_{elst} is not yet converged in double- ζ basis sets even for the S66 dimers, the variations in E_{elst} are $\lesssim 0.1$ kcal/mol. Exchange energies (Figure 6c) also vary by only ~ 1 kcal/mol if double- ζ basis sets are excluded from the comparison. In contrast, induction energies (Figure 6d) span a range of ~ 4 kcal/mol in the various triple- and quadruple- ζ basis sets. This analysis

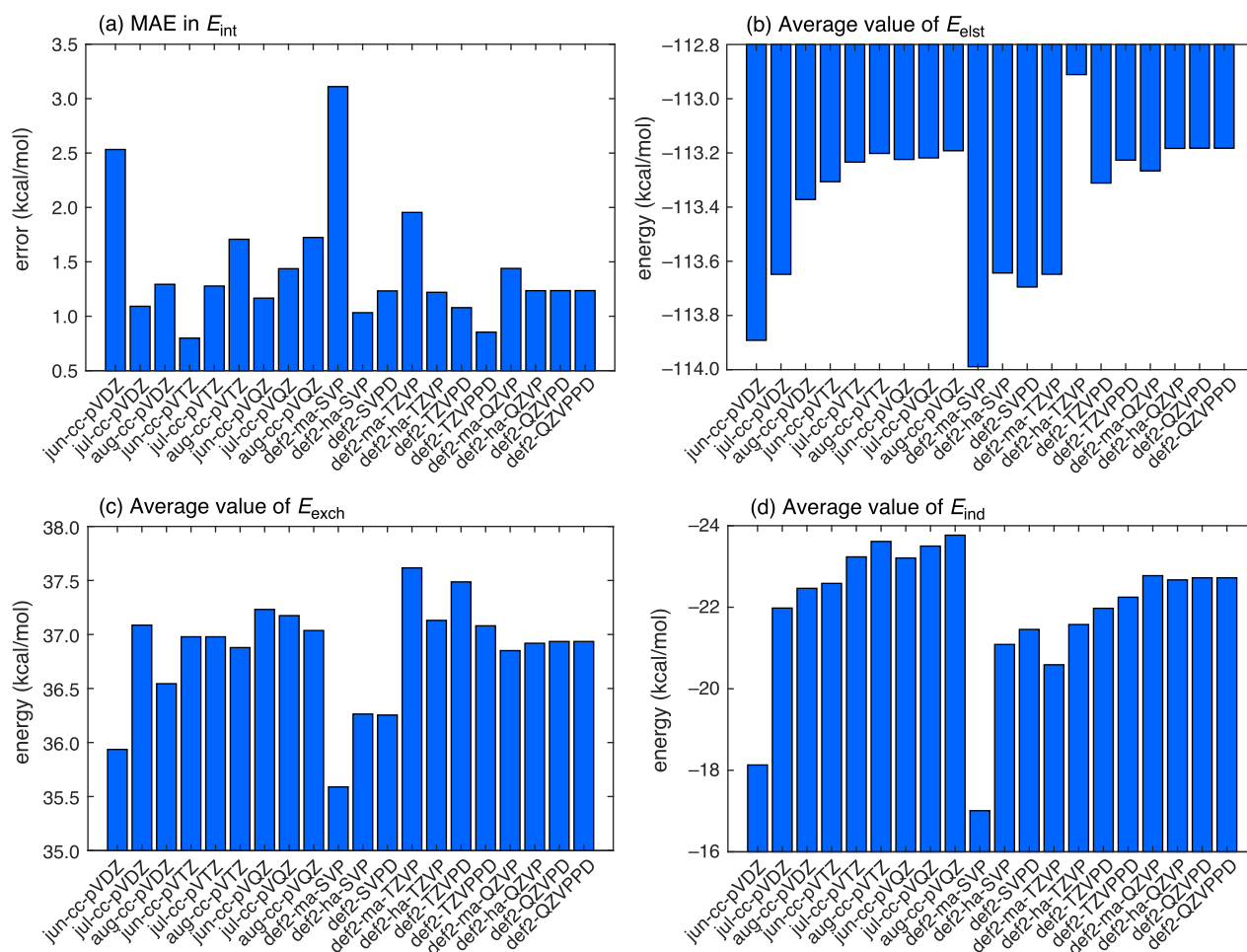


Figure 6. XSAPT + *aiD3* results for the IL16 data set: (a) error in the total interaction energy, and average values of (b) E_{elst} , (c) E_{exch} , and (d) E_{ind} in various basis sets.

points to induction as the energy component wherein the overall errors in the interaction energies reside, which is consistent with the need for a δMP2 correction to achieve sub-kcal/mol accuracy.

In contrast to IL16, overall errors in the interaction energies for the AHB21 and CHB6 data sets follow more discernible and systematic trends; see Table 3. The smallest MAEs (1.2–1.5 kcal/mol) are obtained using the aug-cc-pVQZ and def2-QZVPD basis sets. Trimming the diffuse functions at the triple- ζ level has a noticeably detrimental effect on the anion–neutral dimers in the AHB21 data set. This effect, which was not seen in dimers of neutral molecules, is less evident at the quadruple- ζ level. In general, the basis-set demands for these ion-containing dimers are more severe than they are for the S22 and S66 dimers.

4.6. Halide–Water Clusters. For the S66 data set, we found that induction energies exhibit remarkably little basis-set dependence (see Figure 3d), which might simply reflect that the induction energies for these small, charge-neutral dimers are not especially large. That the ionic test systems considered in section 4.5 exhibit somewhat more stringent basis-set requirements comports with this hypothesis. To test this further, we next consider some larger anion–water clusters whose induction energies are more significant.

4.6.1. Aqueous Chloride Ion. We first consider $\text{Cl}^-(\text{H}_2\text{O})_n$ clusters extracted from a molecular dynamics simulation of $\text{Cl}^-(\text{aq})$,¹⁰¹ and which have previously been used to explore

the energetics of ion hydration.⁶⁴ A set of 51 clusters containing an average of $n = 28$ water molecules (representing two solvation shells) was taken from previous work,^{64,101} and we will examine the basis-set effects on the energy components across this trajectory. These calculations are meant to investigate what (if any) cancellation one can expect across a set of similar geometries for the same system, and for the purposes of these calculations, each $\text{Cl}^-(\text{H}_2\text{O})_n$ snapshot is treated as a dimer with Cl^- as one monomer and $(\text{H}_2\text{O})_n$ as the other. As a representative example of a high-throughput application, we examine some very efficient basis sets such as 6-31+G(d) and 6-311+G(d,p) in addition to higher-quality ones such as def2-TZVPD and some intermediate choices as well. Calculations were performed at the XSAPT + *aiD3* level, and δE_{HF} is *not* included in the induction energy for these calculations in the interest of computational expedience. We expect the convergence behavior of the second-order induction terms in eq 2 to be similar to those of δE_{HF} . The first half of the data set is sufficient to exhibit both the minimum and the maximum value of each energy component, so for clarity, only those data are shown in Figure 7.

While there are certainly systematic errors in particular basis sets, we observe that the overall step-to-step fluctuations (both in E_{int} and in its components) are very similar across basis sets ranging in quality from 6-31+G(d) to def2-TZVPD. Systematic errors are different in various energy components, and this leads to some error cancellation such that E_{int} computed at the

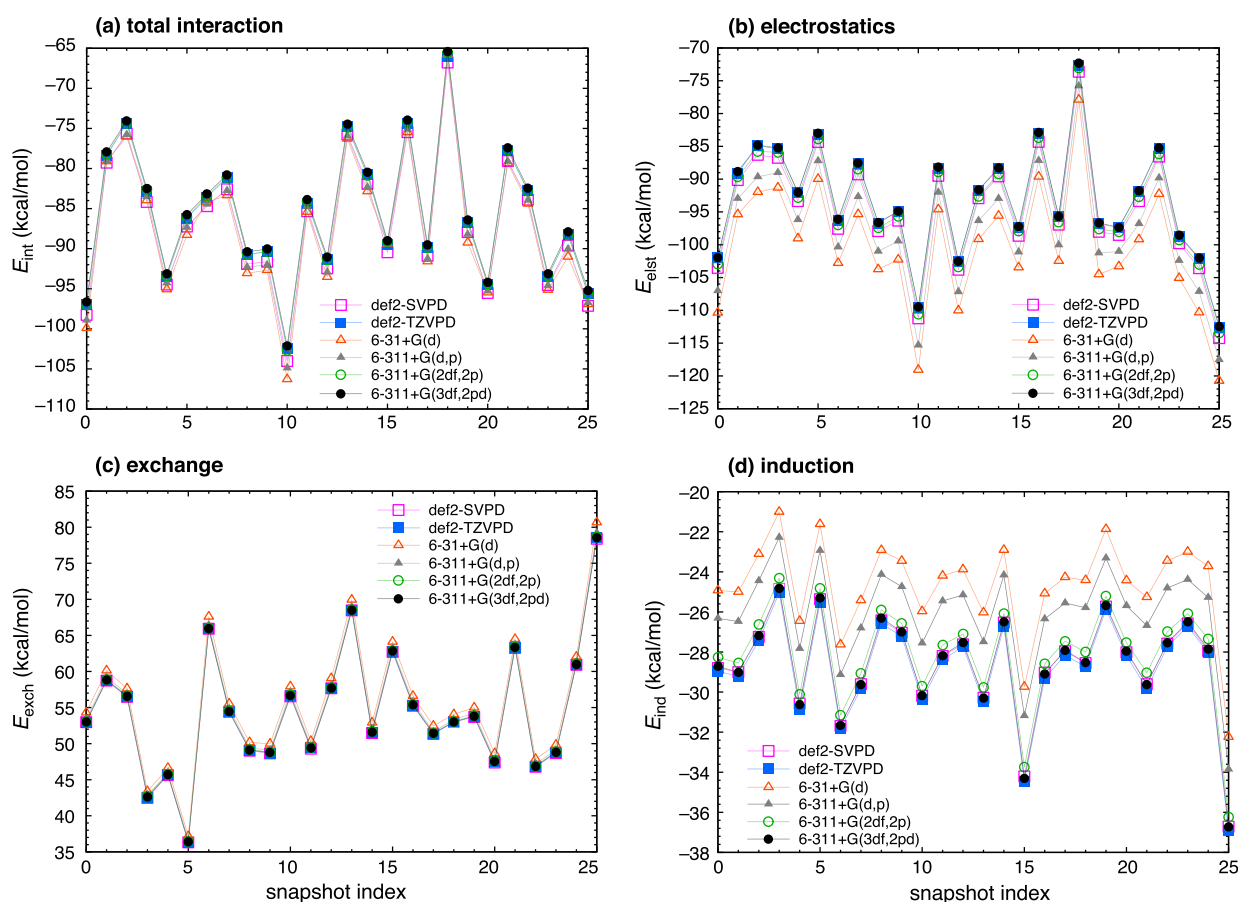


Figure 7. XSAPT + *aiD3* calculations along a Cl^- (aq) trajectory with two solvation shells of explicit water: (a) E_{int} (b) E_{elst} (c) E_{exch} , and (d) E_{ind} . Note that the energy scales are different in each panel. The induction energy contains the second-order terms only and omits δE_{HF} in eq 2.

Table 4. Timing Data and Error Statistics for XSAPT + *aiD3* Calculations on $\text{Cl}^-(\text{H}_2\text{O})_n$

basis set	E_{int} error (kcal/mol) ^b		time (s) ^c	
	MAE ^d	max	CPU	wall
6-31+G(d)	1.9 ± 0.8	3.8	1954	152
6-311+G(d,p)	1.3 ± 0.5	2.4	4912	402
6-311+G(2df,2p)	0.1 ± 0.1	0.4	14 935	1143
6-311+G(3df,2pd)	0.3 ± 0.1	0.6	32 916	2501
def2-SVPD	1.2 ± 0.2	1.5	22 492	2144
def2-TZVPD	0.0	0.0	73 063	6326

^aData represent averages over 51 snapshots with $\langle n \rangle = 28.4 \pm 2.4$ water molecules treated as a single fragment. ^bWith respect to the def2-TZVPD value. ^cCalculations run on 14 processors. ^dUncertainty represents one standard deviation.

XSAPT + *aiD3*/6-31+G(d) level differs from the corresponding def2-TZVPD value by only 1.9 ± 0.8 kcal/mol. This is just 2% of the ensemble-averaged interaction energy, $\langle E_{\text{int}} \rangle = -87.0$ kcal/mol. Error statistics for E_{int} with respect to XSAPT + *aiD3*/def2-TZVPD values that represent our best estimates for this system, are listed in Table 4 along with timing data for various basis sets.

Examining the individual energy components in Figure 7, we note that the relatively low-quality 6-31+G(d) and 6-311+G(d,p) basis sets both overestimate E_{elst} (making it too attractive) but underestimate E_{ind} (making it insufficiently attractive). Partial cancellation of these errors is responsible for the reasonable interaction energies that are obtained in either

basis set. Errors in both E_{elst} and E_{ind} are larger for 6-31+G(d), which therefore relies more heavily on error cancellation. In contrast, the 6-311+G(3df,2pd) basis set affords individual energy components that are fully converged with respect to def2-TZVPD values, so the accuracy of this approach does not rely on error cancellation, and in fact the maximum deviation with respect to the def2-TZVPD interaction energies is only 0.4 kcal/mol when this high-quality Pople basis set is used. Interestingly, the exchange energies appear to be converged in any triple- ζ basis set but also in def2-SVPD, although they are somewhat overestimated when 6-31+G(d) is used.

Timing data in Table 4 demonstrate that the use of 6-311+G(3df,2pd) affords a 2 \times speedup relative to def2-TZVPD. Interestingly, the latter actually comprises fewer basis functions. For $\text{Cl}^-(\text{H}_2\text{O})_{28}$, which is the average size of the clusters examined in this section, the use of def2-TZVPD involves 1670 basis functions versus 1923 for 6-311+G(3df,2pd). The smaller timings for the larger calculation provides an unambiguous indication of the much better efficiency of Pople basis sets, provided that the integrals engine can exploit *sp* shells.

If one removes some of the polarization functions from the highest quality Pople basis set, to obtain 6-311+G(2df,2p), the speedup relative to def2-TZVPD increases to 5 \times while preserving the accuracy of E_{int} at the expense of introducing a small amount of error cancellation between E_{elst} and E_{ind} . This basis is superior to def2-SVPD in both accuracy and efficiency. Nevertheless, it is worth noting that the error in the 6-31+G(d) calculations appears to be quite systematic while

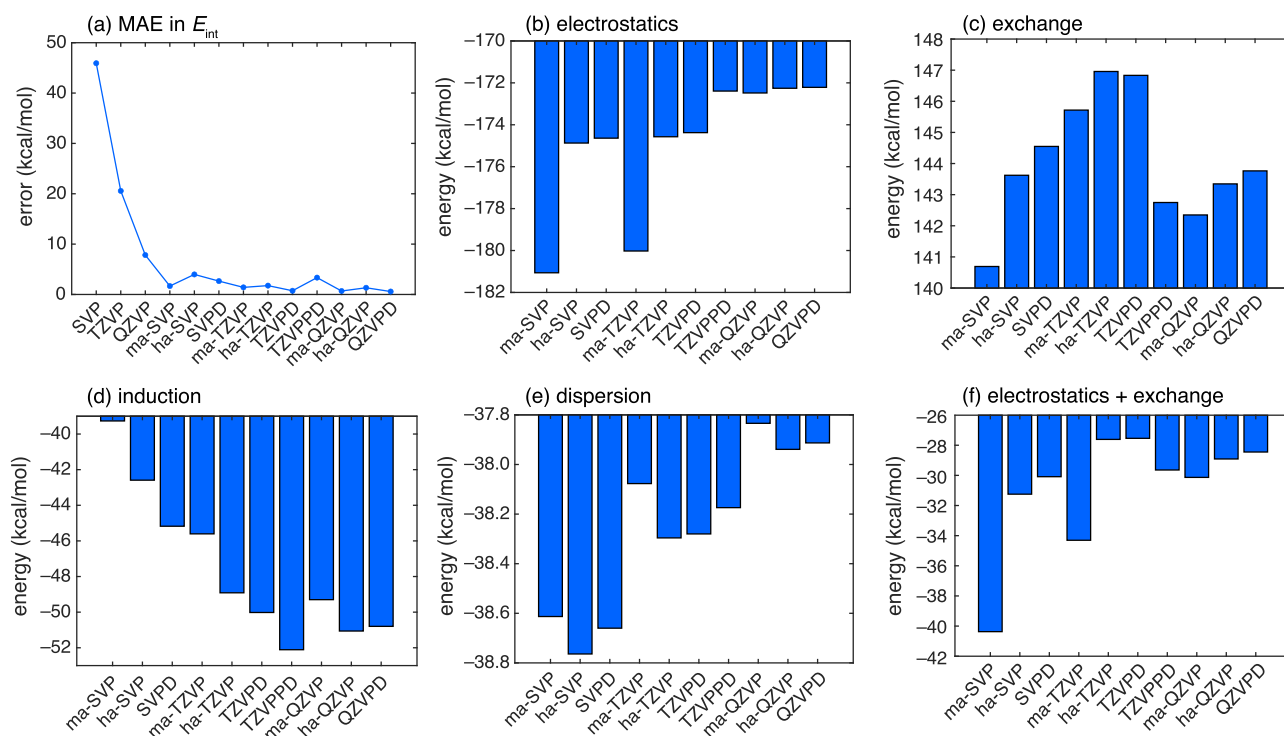


Figure 8. Basis-set dependence of XSAPT + MBD for $F^-(H_2O)_6$ using Karlsruhe basis sets: (a) Errors in E_{int} versus the CCSD(T)/CBS benchmark ($E_{\text{int}} = -116.6$ kcal/mol),¹⁰² and convergence of (b) E_{elst} , (c) E_{exch} , (d) E_{ind} , (e) E_{disp} , and (f) $E_{\text{elst}} + E_{\text{exch}}$ as a function of basis set. For brevity, the “def2” prefix is omitted from the basis-set names. Note also that the basis-set selection (and the ordering) is different in panel a as compared to the other panels in order to highlight the significant errors obtained in the absence of diffuse functions.

affording a speedup of $37\times$ relative to def2-TZVPD. The more affordable Pople basis sets therefore offer good insight as to how the energy components change as a function of geometry in large systems.⁶⁴

4.6.2. Basis-Set Convergence for $F^-(H_2O)_6$. In a similar vein, we next examine the energy components for $F^-(H_2O)_6$, for which CCSD(T)/CBS benchmarks¹⁰² allow us to characterize absolute errors in the interaction energies. In contrast to the $Cl^-(aq)$ system, where each $Cl^-(H_2O)_n$ cluster was treated as a dimer, here we exploit the many-body power of XSAPT to describe $F^-(H_2O)_6$ as a system of 7 fragments.

Figure 8a shows the errors in E_{int} using XSAPT + MBD in various Karlsruhe basis sets. Errors are unacceptably large in the absence of diffuse functions (even using def2-QZVP), which is not surprising, but minimal augmentation is sufficient to reduce the errors to ≤ 5 kcal/mol versus a CCSD(T)/CBS reference energy $E_{\text{int}} = -116.6$ kcal/mol,¹⁰² even at the double- ζ level. In quadruple- ζ basis sets with diffuse functions, the XSAPT + MBD errors are all ≤ 1.3 kcal/mol.

Examining the basis-set convergence of the $F^-(H_2O)_6$ energy components, we find that electrostatic energies (Figure 8b) span a wide range, but if the minimally augmented basis sets are excluded then all of the values of E_{elst} lie between -175 and -172 kcal/mol. At the triple- ζ level, it appears that diffuse functions can safely be deleted from the hydrogen atoms, as the def2-ha-TZVP and def2-TZVP values of E_{elst} differ by only 0.2 kcal/mol. The def2-TZVPD value ($E_{\text{elst}} = -174.4$ kcal/mol) differs by 2 kcal/mol from the def2-QZVPD value ($E_{\text{elst}} = -172.2$ kcal/mol), and in fact the def2-SVPD value is much closer: $E_{\text{elst}} = -174.6$ kcal/mol. As we observed for S66, a double- ζ basis set with a full complement of diffuse functions

can stand in for a triple- ζ basis set for electrostatics calculations.

Exchange energies (Figure 8c) span a similarly wide range and here the diffuse functions are important to prevent severe underestimation of E_{exch} caused by the tails of the anion’s wave function. The def2-SVPD value ($E_{\text{exch}} = 144.6$ kcal/mol) is only about 1 kcal/mol different from the def2-QZVPD value ($E_{\text{exch}} = 143.8$ kcal/mol). Often the sum $E_{\text{elst}} + E_{\text{exch}}$ is easier to interpret than either of these energy components alone,^{36,64} in part because the sum tends to be more comparable to values of $|E_{\text{ind}}|$ and $|E_{\text{disp}}|$, whereas $|E_{\text{elst}}|$ and E_{exch} are individually much larger. Data for $E_{\text{elst}} + E_{\text{exch}}$ in $F^-(H_2O)_6$ are presented in Figure 8f. Using heavy-augmented basis sets, this sum appears to converge at the triple- ζ level, where the difference with respect to def2-QZVPD is only 0.8 kcal/mol, which once again suggests that diffuse functions on hydrogen are not essential at the triple- ζ level. With a full complement of diffuse functions, the def2-SVPD basis set can be substituted for the triple- ζ one with $\lesssim 1$ kcal/mol loss in accuracy.

Induction energies for $F^-(H_2O)_6$ are presented in Figure 8d, and the def2-QZVPD value is $E_{\text{ind}} = -50.8$ kcal/mol. Double- ζ basis sets grossly underestimate this value, even with a full complement of diffuse functions; the def2-SVPD value is $E_{\text{ind}} = -45.2$ kcal/mol, which represents 11% error with respect to the def2-QZVPD value. In contrast, the def2-TZVPD value ($E_{\text{ind}} = -50.0$ kcal/mol) represents an underestimate of 0.8 kcal/mol or 2%. To obtain converged results, triple- ζ basis sets with diffuse functions are required and here the hydrogen atom diffuse functions contribute 1.0 kcal/mol, comparing def2-ha-TZVP to def2-TZVPD.

It is also abundantly clear that the dispersion energy is not very sensitive to the basis set and changes by only 0.7 kcal/mol

Table 5. Error Statistics for SAPT0(HF) + MBD Applied to the S66 Data Set

method	error (kcal/mol)							
	H bonded		dispersion		mixed		all S66	
	MAE	max	MAE	max	MAE	max	MAE	max
def2-SVP	5.24	12.53	2.77	6.73	2.39	3.31	3.52	12.53
def2-SVPD	3.11	8.70	2.28	5.43	1.92	2.95	2.46	8.70
def2-TZVP	2.45	5.38	1.12	3.71	1.44	2.33	1.61	5.38
def2-TZVPD	1.73	4.85	1.06	3.36	1.21	2.07	1.34	4.85
def2-QZVP	2.01	5.88	1.04	3.24	1.24	2.17	1.44	5.88
def2-QZVPD	1.91	5.72	1.04	3.12	1.20	2.09	1.39	5.72
cc-pVDZ	4.86	11.84	2.81	6.73	2.46	3.46	3.42	11.84
jun-cc-pVDZ	3.52	8.93	1.64	4.68	1.61	2.48	2.29	8.93
jul-cc-pVDZ	2.02	5.77	1.06	3.40	1.19	2.07	1.44	5.77
aug-cc-pVDZ	2.63	7.22	1.68	4.43	1.61	2.41	1.99	7.22
cc-pVTZ	3.43	8.38	1.69	4.76	1.82	2.80	2.34	8.38
jun-cc-pVTZ	2.28	6.28	1.27	3.97	1.29	2.06	1.63	6.28
jul-cc-pVTZ	2.29	6.29	1.28	3.86	1.31	2.07	1.64	6.29
aug-cc-pVTZ	2.30	6.41	1.23	3.80	1.26	2.07	1.61	6.41
cc-pVQZ	2.32	6.09	1.17	3.72	1.42	2.43	1.64	6.09
jun-cc-pVQZ	1.98	5.65	1.06	3.35	1.20	2.08	1.43	5.65
jul-cc-pVQZ	2.02	5.77	1.06	3.40	1.19	2.07	1.44	2.07
aug-cc-pVQZ	1.98	5.83	1.07	3.39	1.20	2.04	1.43	5.83
6-311+G(3df,2pd)	2.92	8.40	1.56	4.49	1.53	2.41	2.02	8.40
6-311++G(3df,2pd)	2.90	8.37	1.59	4.52	1.58	2.46	2.04	8.37

Table 6. Error Statistics for SAPT0(KS) + MBD Applied to the S66 Data Set^a

method	error (kcal/mol)							
	H bonded		dispersion		mixed		all S66	
	MAE	max	MAE	max	MAE	max	MAE	max
def2-SVP	3.56	7.38	2.39	5.37	1.84	2.52	2.60	7.38
def2-SVPD	0.67	1.92	1.66	3.47	1.19	2.25	1.17	3.47
def2-TZVP	0.40	0.95	0.58	2.02	0.79	1.35	0.58	2.02
def2-TZVPD	0.50	1.62	0.43	1.51	0.48	0.95	0.47	1.62
def2-QZVP	0.22	0.77	0.38	1.30	0.53	1.11	0.37	1.30
def2-QZVPD	0.43	0.98	0.32	1.00	0.46	1.10	0.40	1.10
cc-pVDZ	3.13	6.90	2.45	5.37	1.89	2.61	2.52	6.90
jun-cc-pVDZ	0.81	1.96	0.72	2.06	0.67	1.32	0.74	2.06
jul-cc-pVDZ	0.31	1.01	0.76	2.06	0.62	1.27	0.56	2.06
aug-cc-pVDZ	0.19	0.81	0.77	2.02	0.68	1.45	0.54	2.02
cc-pVTZ	1.74	3.55	1.17	3.20	1.19	1.73	1.38	3.55
jun-cc-pVTZ	0.17	0.60	0.55	1.79	0.49	1.00	0.40	1.79
jul-cc-pVTZ	0.16	0.60	0.53	1.65	0.49	1.01	0.39	1.65
aug-cc-pVTZ	0.21	0.67	0.42	1.53	0.41	1.00	0.34	1.53
cc-pVQZ	0.36	0.66	0.59	2.10	0.76	1.40	0.56	2.10
jun-cc-pVQZ	0.39	1.01	0.31	1.04	0.42	0.95	0.37	1.04
jul-cc-pVQZ	0.34	0.92	0.31	1.10	0.40	0.91	0.35	1.10
aug-cc-pVQZ	0.42	0.87	0.28	1.05	0.38	0.95	0.36	1.05
6-311+G(3df,2pd)	0.56	2.05	0.86	2.41	0.79	1.41	0.73	2.41
6-311++G(3df,2pd)	0.50	1.95	0.81	2.34	0.74	1.40	0.68	2.34

^aSee Table S10 for comparison to values that exclude the δE_{HF} correction.

between the def2-ma-SVP and the def2-QZVPD basis sets. This is consistent with earlier results for other data sets where the dispersion energy is nearly constant across a wide range of basis sets, suggesting that MBD gives both accurate dispersion energies and ones that converge quickly.

4.7. Performance of Different SAPT Methods. In this section, we compare the performance of three different SAPT variants [XSAPT, SAPT0(HF), and SAPT0(KS)], using either MBD or *aiD3* to replace second-order dispersion (eq 3) in

each case. The purpose of these tests is to examine the importance of the self-consistent XPol charge embedding that is used in XSAPT + MBD, thus the two SAPT0 variants do not include such an embedding. The SAPT0(HF) + MBD method consists of a standard HF-based SAPT0 calculation but with a modified dispersion term, while SAPT0(KS) + MBD uses GDD-tuned LRC- ω PBE in place of HF theory for the monomer wave functions and is therefore similar to XSAPT + MBD except that the self-consistent embedding is omitted.

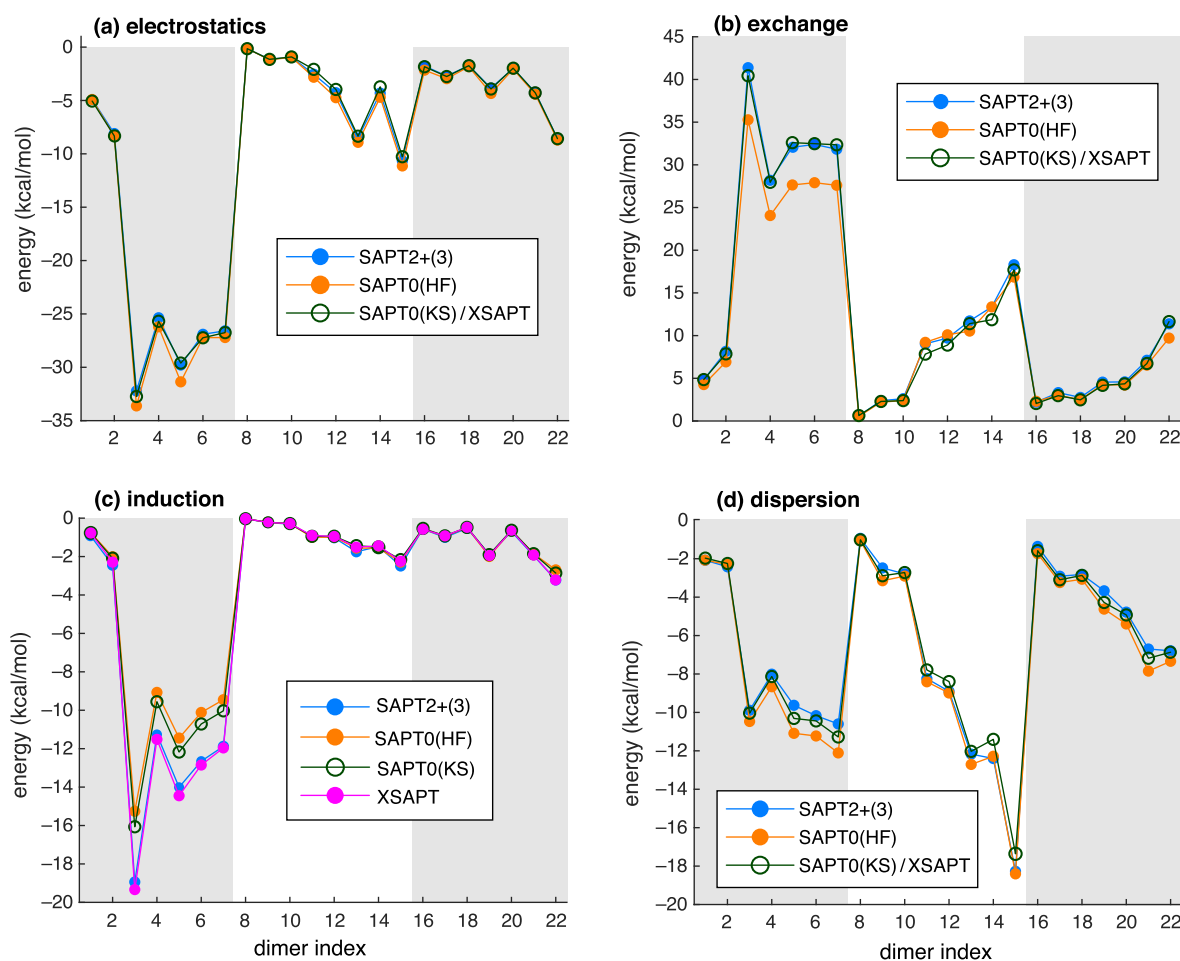


Figure 9. Comparison of energy components for the S22 set of dimers: (a) E_{elst} , (b) E_{exch} , (c) E_{ind} , and (d) E_{disp} . Benchmark SAPT2+(3) results using the aug-cc-pVTZ data set are taken from ref 93, whereas SAPT0(HF) + MBD, SAPT0(KS) + MBD, and XSAPT + MBD calculations were performed using the aug-cc-pVQZ basis set. The latter two methods are indistinguishable except for E_{ind} in panel c. Shaded regions delineate the electrostatics-dominated dimers (1–7), dispersion-dominated dimers (8–15), and dimers with mixed-influence interactions (16–22). Note that the energy scale is different in each panel.

4.7.1. Total Interaction Energies. Error statistics for the SAPT0(HF) + MBD and SAPT0(KS) + MBD methods, as applied to the S66 dimers data set, are provided in Tables 5 and 6, respectively, which should be compared to the statistics for XSAPT + MBD that are listed in Table 2. SAPT0(HF) + MBD is clearly less accurate than either of the approaches based on LRC- ω PBE for the monomers, with MAEs that are consistently 1.0–1.5 kcal/mol larger. (This is analyzed in terms of energy components in section 4.7.2.) Statistically speaking, the performance of SAPT0(KS) + MBD and XSAPT + MBD is about the same for these dimers. For a dimer, the difference between these two methods is the self-consistent XPol charge embedding, which is not expected to have a significant effect in a dimer because many-body polarization is absent by definition. This comparison simply serves as a baseline test to indicate that charge embedding does not improve the quality of the zeroth-order wave function in any statistically meaningful way, at least for small dimers.

Recall that the δE_{HF} correction is included in all calculations reported in this work except where explicitly indicated otherwise. Table S10 juxtaposes the SAPT0(KS) + MBD results from Table 6, which include this correction, with error statistics obtained when δE_{HF} is omitted. Without this correction, the errors are *significantly* larger for hydrogen-

bonded complexes (as seen in previous work),⁴² except in double- ζ basis sets where there is fortuitous error cancellation. For the dispersion-dominated and mixed-influence subsets of S66, however, both the average and the maximum errors are actually slightly smaller when the δE_{HF} correction is omitted, although the differences are small enough that the overall error statistics improve upon addition of this correction.

Error statistics for the ion-containing data sets are provided in Tables S11, S12, and S13, computed with the *aiD3* versions of XSAPT, SAPT0(HF), and SAPT0(KS). Here the trend is different, and XSAPT + *aiD3* outperforms both of the other methods by 1–2 kcal/mol for the IL16 data set and by a lesser amount for the AHB21 data set. The fact that XSAPT + *aiD3* exhibits statistically significant error reduction as compared to SAPT0(KS) + *aiD3* suggests that induction effects are large enough in these systems so that the charge-embedded XPol determinant is a better reference state for perturbation theory as compared to the use of isolated monomer wave functions.

In contrast to the behavior for IL16 and AHB21, where XSAPT + *aiD3* appears to offer a clear improvement over the other two *aiD3* methods, results from all three approaches are much more similar for the CHB6 data set (see Table S13). This data set consists of $M^+(\text{H}_2\text{O})$ and $M^+(\text{C}_6\text{H}_6)$ complexes with $M = \text{Li}, \text{Na}, \text{or K}$. Specifically for the cations, the tuning

Table 7. Error Statistics for Energy Components in the S22 Data Set^a

method	subset	error (kcal/mol)							
		electrostatics		exchange		induction		dispersion	
		MAE	max	MAE	max	MAE	max	MAE	max
SAPT0(HF) + MBD	elst.	0.72	1.57	3.59	6.10	2.00	3.68	0.77	1.51
SAPT0(HF) + MBD	disp.	0.26	0.48	0.45	1.45	0.08	0.20	0.24	0.67
SAPT0(HF) + MBD	mixed	0.23	0.50	0.51	1.45	0.12	0.53	0.60	1.15
SAPT0(HF) + MBD	all	0.40	1.57	1.47	6.10	0.70	3.68	0.53	1.51
SAPT0(KS) + MBD	elst.	0.27	0.52	0.38	0.95	1.53	2.88	0.31	0.68
SAPT0(KS) + MBD	disp.	0.25	0.59	0.60	1.50	0.10	0.33	0.44	1.00
SAPT0(KS) + MBD	mixed	0.04	0.08	0.29	0.38	0.10	0.36	0.25	0.61
SAPT0(KS) + MBD	all	0.19	0.59	0.45	1.50	0.62	2.88	0.35	1.00
XSAPT + MBD	elst.	0.27	0.52	0.38	0.95	0.24	0.44	0.31	0.68
XSAPT + MBD	disp.	0.25	0.59	0.60	1.50	0.08	0.25	0.44	1.00
XSAPT + MBD	mixed	0.04	0.08	0.29	0.38	0.04	0.08	0.25	0.61
XSAPT + MBD	all	0.19	0.59	0.45	1.50	0.12	0.44	0.35	1.00

^aError is relative to SAPT2+(3)/aug-cc-pVTZ benchmarks from ref 93.

procedure affords rather large values of ω_{GDD} (Table S4): $\omega_{\text{GDD}} = 1.30 a_0^{-1}$, $0.84 a_0^{-1}$, and $0.59 a_0^{-1}$ for Li^+ , Na^+ , and K^+ , respectively. The values for Li^+ and Na^+ are much larger than the tuned values for small, charge-neutral monomers or anions, and even the value obtained for K^+ is somewhat larger than what we observe for other systems. The range separation in LRC- ω PBE occurs at a distance of $\approx \omega_{\text{GDD}}^{-1}$, and that value corresponds to 0.41 Å for Li^+ , 0.63 Å for Na^+ , and 0.90 Å for K^+ . In each case, this is smaller than the van der Waals radius of the cation itself,¹⁰³ meaning that for the purpose of intermolecular interactions computations, the XSAPT + *aiD3* calculations are using HF theory for the exchange functional. This explains the close similarity with SAPT0(HF) + *aiD3*.

4.7.2. Energy Components. To further investigate these three variants of SAPT and to understand the origins of the differences between them, we next examine individual energy components. For this we turn to the S22 data set,⁹² for which benchmark energy components are available,⁹³ computed at the SAPT2+(3)/aug-cc-pVTZ level. Figure 9 compares benchmarks against the SAPT0(HF) + MBD, SAPT0(KS) + MBD, and XSAPT + MBD methods, and Table 7 lists the error statistics in each energy component. These data indicate that E_{exch} and E_{ind} for the electrostatically dominated subset of S22, are responsible for the diminished accuracy of SAPT0(HF) + MBD relative to other methods; these two components exhibit MAEs of 3.6 and 2.0 kcal/mol, respectively, for the subset that includes the hydrogen-bonded dimers.

For the DFT-based second-order methods, most of the energy components exhibit sub-kcal/mol MAEs, with the lone exception being E_{ind} for the electrostatically dominated dimers described at the SAPT0(KS) + MBD level, for which the MAE is 1.5 kcal/mol. That is reduced to 0.2 kcal/mol using XSAPT + MBD, demonstrating the importance of charge embedding even in a dimer system, at least where hydrogen bonds are concerned. For the dimers that are not dominated by electrostatics, charge embedding makes little difference and the error statistics for both SAPT0(KS) + MBD and XSAPT + MBD are very similar for each energy component. Notably, error statistics for the induction energy evaluated using SAPT0(KS) + MBD are more similar to the SAPT0(HF) + MBD errors than they are to the XSAPT + MBD errors. Each of these methods uses the same δE_{HF} correction (evaluated in each case using HF theory and not DFT), which again

supports the important role that charge embedding plays even in dimers, at least where hydrogen bonds are involved. Swapping DFT for HF orbitals reduces the MAE for the hydrogen-bonded subset from 2.0 to 1.5 kcal/mol; adding charge embedding reduces it even more to 0.2 kcal/mol.

4.8. Mixed-Basis Calculations. We now consider the possibility of a hybrid method in which different energy components are computed with different basis sets, exploiting the separability of the SAPT decomposition. A simple-to-implement version of such a procedure is to focus on the δE_{HF} correction, which requires a dimer HF calculation. This is the only part of an XSAPT calculation that requires an iterative SCF calculation on something larger than a monomer, and it is usually the computational bottleneck step when large basis sets are employed. That δE_{HF} is defined by difference (eq 4) also suggests that this term might converge more rapidly than other energy components in eq 1, similar to the way that a correction $\delta = E_{\text{CCSD(T)}} - E_{\text{MP2}}$ converges more rapidly than either $E_{\text{CCSD(T)}}$ or E_{MP2} .¹⁰⁴

To test this, we repeated the XSAPT + MBD calculations on the S66 dimers using the def2-QZVPD basis set to evaluate all of the terms in eq 1 except for δE_{HF} , for which we use a smaller basis set. The smaller basis set is used both for the supramolecular HF calculation (for $\Delta E_{\text{int}}^{\text{HF}}$) and to solve the coupled-perturbed equations that are used to obtain $E_{\text{ind, resp}}^{(2)} + E_{\text{exch-ind, resp}}^{(2)}$ in eq 4. Table 8 shows the error statistics for this mixed-basis scheme, averaged over the S66 data set and using various choices for the smaller (δE_{HF}) basis set, and Figure S4 shows the individual errors across S66 for a selection of basis sets. Even when δE_{HF} is evaluated with a basis set as small as 6-31G*, the errors (with respect to the full def2-QZVPD result) are uniformly <1 kcal/mol. Average errors with respect to the CCSD(T)/CBS benchmarks using def2-QZVPD for all of the terms except δE_{HF} are all ≈ 0.4 kcal/mol (see Table 8), using a variety of small basis sets to evaluate δE_{HF} .

Timing data for these mixed-basis calculations are shown in Figure 10 using the largest of the S66 systems, uracil dimer. These data demonstrate the dramatic speedups that are afforded by this simple hybrid procedure. If δE_{HF} is evaluated using def2-ma-SVPD or 6-31+G(d), with all other parts of the calculation performed using def2-QZVPD, then the total cost of the calculation is reduced by 3.8×. This substitution introduces an error of <0.1 kcal/mol. The speedup can be

Table 8. Accuracy of XSAPT + MBD/def2-QZVPD for the S66 Data Set Using a Smaller Basis for δE_{HF}

basis set for δE_{HF}	MAE (kcal/mol)	
	vs CCSD(T)/CBS ^a	vs XSAPT + MBD/def2-QZVPD ^b
6-31G(d)	0.36	0.12
6-31+G(d)	0.37	0.06
def2-ma-SVP	0.36	0.11
def2-ha-SVP	0.38	0.07
def2-SVPD	0.38	0.07
def2-ma-TZVP	0.39	0.03
def2-ha-TZVP	0.40	0.02
def2-TZVPD	0.40	0.02
def2-ma-QZVP	0.40	0.00
def2-ha-QZVP	0.40	0.00

^aMAE with respect to the CCSD(T)/CBS benchmark value of E_{int} .

^bMAE with respect to conventional XSAPT + MBD/def2-QZVPD.

expected to improve as the system size increases, since the cost of the δE_{HF} correction scales with dimer size whereas other parts of the XSAPT procedure scale only with monomer size, meaning that the δE_{HF} calculation will constitute an increasing fraction of the total cost as the system grows larger. This will be evident in the timing data presented below for much larger supramolecular complexes.

4.9. Results for Large Complexes. To complement the small dimer and cluster systems examined above, we next present two examples of XSAPT + MBD calculations on much larger systems: coronene dimer ($\text{C}_{24}\text{H}_{12}$)₂, which is one of the dispersion-bound systems in the L7 data set,⁹⁰ and a DNA–ellipticine intercalation complex,¹⁰⁵ which has become something of a standard test system in noncovalent quantum chemistry.^{20,58,60,106–108} The latter system contains 157 atoms including the ligand (ellipticine), two hydrogen-bonded base pairs, and the sugar/phosphate backbone. In the calculations presented below, the 33-atom ligand is treated as one monomer and the entire double-stranded DNA model as a second monomer (with 124 atoms and -2 charge).

These two systems are interesting in part because there is a discrepancy in both cases between the various benchmark interaction energies available in the literature. For the DNA intercalation complex, a recent CCSD(T)/CBS benchmark

($E_{\text{int}} = -38.0 \pm 2.2$ kcal/mol¹⁰⁸) is inconsistent with an older quantum Monte Carlo (QMC) estimate ($E_{\text{int}} = -33.6 \pm 0.9$ kcal/mol¹⁰⁷), even after accounting for the reported uncertainties in both values. For coronene dimer, the QMC benchmark ($E_{\text{int}} = -18.1 \pm 0.8$ kcal/mol¹⁰⁹) and the CCSD(T)/CBS benchmark ($E_{\text{int}} = -20.93 \pm 0.44$ kcal/mol¹⁰⁸) remain 1.6 kcal/mol apart after accounting for the uncertainties, although the smaller uncertainty in the CCSD(T)/CBS value in this case means that the two values of E_{int} are not so far apart as they are for the DNA intercalation complex. A few other examples where QMC and CCSD(T)/CBS benchmarks are inconsistent with one another have also been reported recently,^{109,110} and it is unclear to us which values are more reliable. QMC calculations are subject to an unknown fixed-node error that is not reflected in the statistical uncertainty, while CCSD(T)/CBS calculations on systems of this size are presently only tractable within the domain-localized pair natural orbital (DLPNO) approximation.^{111–113}

For noncovalent interactions, this approximation is especially sensitive to numerical thresholds,¹¹⁴ although this has been taken into consideration in the benchmark calculations cited above. The accuracy of the DLPNO approximation is also sensitive to the system size.¹¹⁵

For these large systems, the δE_{HF} correction is the most time-consuming part of an XSAPT calculation and the mixed-basis approach introduced above stands to yield considerable savings. We therefore benchmark this approach for these larger systems using a variety of small basis sets to evaluate δE_{HF} (see Table 9). With only one exception, errors in δE_{HF} are ≤ 0.3 kcal/mol for each of the smaller basis sets that we test, as measured with respect to the value computed in the largest basis set that is practical in either case. The one slightly larger error (of 0.5 kcal/mol) occurs when def2-SVP is used to evaluate δE_{HF} for the DNA–ellipticine complex. Given the -2 charge on the DNA backbone, this would seem to be an inappropriate choice and is included here mostly for completeness, although it is interesting that the δE_{HF} error remains rather small even in the absence of any diffuse functions at all. On the basis of these tests, we recommend 6-31+G(d) for the δE_{HF} correction, as the error is < 0.3 kcal/mol and this basis is much more efficient than any of the others that are listed in Table 9.

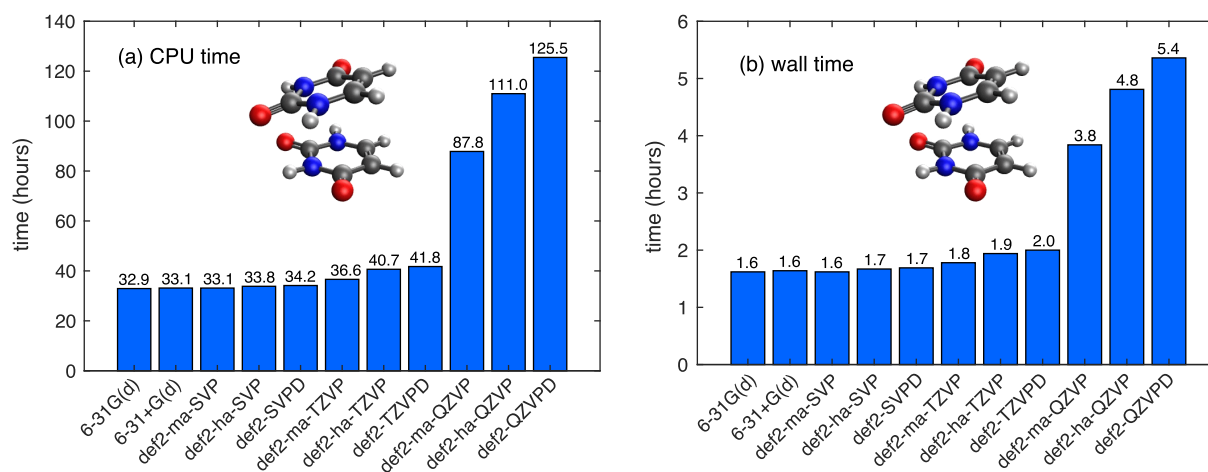


Figure 10. Total (a) CPU time and (b) wall time for a XSAPT + MBD/def2-QZVPD calculation of uracil dimer (shown) using a mixed-basis approach in which the δE_{HF} correction is evaluated using a smaller basis set (as indicated). All calculations were performed on a single 28-core node, and time (in hours) is indicated at the top of each bar.

Table 9. Accuracy of the Mixed-Basis δE_{HF} Approach for Large Complexes^a

basis set for δE_{HF}	(coronene) ₂		DNA/ellipticine	
	δE_{HF}	error ^b	δE_{HF}	error ^c
6-31+G(d)	-1.82	0.24	-2.90	0.27
6-311+G(3df,2pd)	-2.04	0.03	-3.15	0.01
6-311++G(3df,2pd)	-2.04	0.03	-3.15	0.01
def2-SVP	-1.75	0.31	-2.63	0.53
def2-ma-SVP	-1.79	0.30	-2.70	0.47
def2-ha-SVP	-1.77	0.29	-2.87	0.29
def2-SVPD	-1.77	0.30	-2.87	0.29
def2-TZVP	-2.04	0.03	-3.24	0.07
def2-ma-TZVP	-2.05	0.02	-3.25	0.09
def2-ha-TZVP	-2.06	0.01	-3.28	0.12
def2-TZVPD	-2.06	0.01	-3.16	0.00
jun-cc-pVDZ	-1.99	0.08	-3.07	0.05
jul-cc-pVDZ	-2.00	0.06	-3.21	0.04
aug-cc-pVDZ	-2.00	0.07	-3.22	0.10
jun-cc-pVTZ	-2.06	0.01	-3.17	0.004
jul-cc-pVTZ	-2.06	0.00	<i>d</i>	<i>d</i>

^aAll values are in kcal/mol. ^bWith respect to the def2-ma-QZVP value, $\delta E_{\text{HF}} = -2.07$ kcal/mol. ^cWith respect to the def2-TZVPD value, $\delta E_{\text{HF}} = -3.16$ kcal/mol. ^dOmitted for reasons of cost.

We now turn to total interaction energies for these large complexes, using 6-31+G(d) to evaluate δE_{HF} . (Although we have large-basis benchmarks for δE_{HF} , this allows us to present timing data for realistic applications using the mixed-basis procedure.) Interaction energies and timing data for DNA–ellipticine are presented in Table 10 using a variety of basis sets for the other energy components besides δE_{HF} .

Only the highest quality basis sets that we can afford for this system, def2-TZVPD and jun-cc-pVTZ, afford interaction

Table 10. XSAPT + MBD Results for the DNA–Ellipticine Intercalation Complex

basis set ^a	E_{int} (kcal/mol)		time ^c (h)
	sans δE_{HF}	with δE_{HF} ^b	
6-311+G(3df,2pd)	-43.2	-46.1	603.6
6-311++G(3df,2pd)	-42.6	-45.5	621.0
def2-SVP	-61.3	-64.2	56.6
def2-ma-SVP	-55.7	-58.6	69.3
def2-ha-SVP	-54.1	-57.0	121.4
def2-SVPD	-54.1	-57.0	143.6
def2-TZVP	-42.9	-45.8	199.4
def2-ma-TZVP	-41.1	-44.0	267.7
def2-ha-TZVP	-40.5	-43.4	586.2
def2-TZVPD	-40.4	-43.3	636.7
jun-cc-pVDZ	-43.8	-46.7	133.8
jul-cc-pVDZ	-43.3	-46.2	232.3
aug-cc-pVDZ	-43.2	-46.1	322.1
jun-cc-pVTZ	-40.3	-43.2	995.1
CCSD(T)/CBS ^d	-38.6 ± 2.2		
QMC ^e	-33.6 ± 0.9		

^aCalculations performed at the XSAPT + MBD level (except for the benchmarks) using the indicated basis set for all parts of the calculation except δE_{HF} . ^bThe δE_{HF} calculation is performed using 6-31+G(d). ^cAggregate time on 28 processors including the time to evaluate δE_{HF} , which is 41.2 h in each case. ^dDLPNO-CCSD(T)/CBS value from ref 108. ^eFixed-node diffusion Monte Carlo value from ref 107.

energies that begin to approach the CCSD(T)/CBS benchmark, although even these XSAPT + MBD values are overbound by ≈ 1.7 kcal/mol in the absence of the δE_{HF} correction. When that correction is included ($\delta E_{\text{HF}} = -2.9$ kcal/mol), the XSAPT + MBD interaction energy moves even further away from the CCSD(T)/CBS value and further still from the QMC reference value, which is less strongly bound. Nevertheless, these XSAPT + MBD values with triple- ζ basis sets and including δE_{HF} represent the highest level XSAPT methods that have been applied to this system, and this set of calculations appears to reach a consensus value of $E_{\text{int}} \approx -43.3$ kcal/mol for XSAPT + MBD in the large-basis limit. The origins of the discrepancy with respect to either the DLPNO-CCSD(T)/CBS or the QMC benchmark remain a topic for further investigation.

Analogous XSAPT + MBD results for coronene dimer are presented in Table 11. For the Karlsruhe basis sets, the

Table 11. XSAPT + MBD Results for Coronene Dimer

basis set ^a	E_{int} (kcal/mol)		time ^c (h)
	sans δE_{HF}	with δE_{HF} ^b	
6-311+G(3df,2pd)	-25.8	-27.7	81.6
6-311++G(3df,2pd)	-25.6	-27.5	82.6
def2-ma-SVP	-31.1	-32.9	12.0
def2-ha-SVP	-32.2	-33.9	19.2
def2-SVPD	-32.1	-33.9	22.7
def2-ma-TZVP	-20.5	-22.3	50.4
def2-ha-TZVP	-20.7	-22.5	89.3
def2-TZVPD	-20.8	-22.6	106.8
def2-ma-QZVP	-21.4	-23.3	462.1
def2-ha-QZVP	-21.3	-23.2	750.3
def2-QZVPD	-21.1	-22.9	850.8
jun-cc-pVDZ	-27.2	-29.0	21.1
jul-cc-pVDZ	-26.8	-28.6	37.2
aug-cc-pVDZ	-27.2	-29.0	45.5
jun-cc-pVTZ	-22.4	-24.2	146.8
jul-cc-pVTZ	-22.3	-24.2	316.9
aug-cc-pVTZ	-22.2	-24.0	415.1
CCSD(T)/CBS ^d	-20.93 ± 0.44		
QMC ^e	-18.1 ± 0.8		

^aCalculations performed at the XSAPT + MBD level (except for the benchmarks) using the indicated basis set for all parts of the calculation except δE_{HF} . ^bThe δE_{HF} calculation is performed using 6-31+G(d). ^cAggregate time on 40 processors including the time to evaluate δE_{HF} , which is 7.3 h in each case. ^dDLPNO-CCSD(T)/CBS value from ref 108. ^eFixed-node diffusion Monte Carlo value from ref 109.

difference between minimal and full augmentation is mostly insignificant (equal to 1.0 kcal/mol at the double- ζ level but much smaller in larger basis sets), whereas the difference between jun-cc-pVXZ and aug-cc-pVXZ ($X = \text{D or T}$) is completely insignificant. It is worth noting that jun-cc-pVXZ retains some higher angular momentum diffuse functions beyond minimal augmentation, and these appear to be adequate to afford an interaction energy that is converged with respect to inclusion of further diffuse functions. The calculations appear to converge to a value $|E_{\text{int}}| = 21\text{--}22$ kcal/mol in the absence of the δE_{HF} correction or $|E_{\text{int}}| = 23\text{--}24$ kcal/mol when δE_{HF} is included. The latter value represents what is, in principle, the most complete version of XSAPT + MBD that we have applied to this system yet remains

somewhat overbound with respect to the DLPNO-CCSD(T)/CBS benchmark ($|E_{\text{int}}| = 21$ kcal/mol¹⁰⁸). As in the DNA–ellipticine case, the QMC benchmark is somewhat less strongly bound ($|E_{\text{int}}| = 18$ kcal/mol¹⁰⁹).

For both of the large systems examined in this section, inclusion of the δE_{HF} correction degrades the agreement with the benchmarks. Reasons for this are unclear, although in the absence of hydrogen bonding the δE_{HF} correction also (slightly) degrades the accuracy of SAPT0(KS) + MBD calculations for the S66 dimers (see Table S10). For these larger supramolecular complexes, however, this effect is much larger and amounts to 2–3 kcal/mol. It is worth noting the hybrid nature of the δE_{HF} correction in XSAPT: $E_{\text{ind}}^{(2)} + E_{\text{exch-ind}}^{(2)}$ in eq 2 is computed using DFT (tuned LRC- ω PBE functional), whereas δE_{HF} (eq 4) is computed using HF theory. Although this mixed procedure has been carefully examined in small systems (e.g., in Table S10 and also in ref 42), it is possible that those benchmarks misrepresent the behavior in larger systems. Note that overestimation of the large-system interaction energies is not unique to XSAPT + MBD, as SAPT0(KS) + MBD calculations also exhibit this same behavior and are in fact numerically quite close to the XSAPT + MBD values (see Table S14). As such, this effect cannot be blamed on double counting of induction effects due to the use of charge embedding as no such embedding is used in SAPT0(KS) + MBD. The origin of these discrepancies and the seemingly deleterious effect of δE_{HF} in these large supramolecular complexes remain a topic for further investigation.

Examining the timing data for these large supramolecular complexes (Tables 10 and 11), it is clear that the cost can be reduced substantially by trimming the diffuse functions. For coronene dimer, the change from def2-QZVPD to def2-ma-QZVP is accompanied by a 0.3 kcal/mol (or 1%) increase in the interaction energy and a 2 \times speedup. The change from def2-TZVPD to def2-ma-TZVP also changes the interaction energy by 0.3 kcal/mol and also results in a 2 \times speedup. The “sweet spots” for this system would appear to be def2-TZVPD or jun-cc-pVTZ, for which the interaction energies are within about 1 kcal/mol of the def2-QZVPD result, but the cost is less (in either case) than that associated with def2-ma-QZVP. As applied to the DNA–ellipticine complex, these same two basis sets appear to afford converged results, to the extent that we can tell without prohibitively expensive quadruple- ζ calculations.

In examining lower cost alternatives to def2-TZVPD or jun-cc-pVTZ, it seems that def2-SVPD is wholly inadequate, even if it was able to function as a stand in for triple- ζ basis sets in some small-molecule complexes. The jun-cc-pVDZ basis is better (and 7 \times faster than jun-cc-pVTZ) but overestimates the XSAPT + MBD/jun-cc-pVTZ interaction energy by 3.5 kcal/mol (or 9%) for the DNA complex and by 4.8 kcal/mol (21%) for the coronene dimer.

5. CONCLUSIONS

In this comprehensive assessment of the basis-set behavior for the XSAPT, SAPT0, and SAPT0(KS) methods, we have demonstrated that the energy components E_{elstv} , E_{exch} , E_{ind} , and E_{disp} converge in different ways with respect to the underlying Gaussian basis set. The XSAPT approach^{20,58} replaces conventional second-order dispersion with a model that is both cheaper and more accurate: either MBD,^{59,60} or else *aiD3*.^{48,58} The former is a first-principles, density-dependent

description of dispersion,^{73,74} but one that substantially mitigates the basis-set dependence of E_{disp} as compared to conventional wave function-based descriptions of dispersion. For XSAPT + MBD, the dispersion energy is converged (or nearly converged) already in double- ζ basis sets, while for XSAPT + *aiD3*, the dispersion potential has no basis-set dependence at all. In contrast, for conventional SAPT, DFT-SAPT, or MP2 calculations, E_{disp} exhibits the slowest convergence with respect to basis set among all of the energy components,⁵² which was a motivating factor in the early development of XSAPT.⁵⁶

With the basis-set dependence of E_{disp} rendered manageable, it is no longer clear that a compromise (or “Pauling point”) basis set, such as jun-cc-pVDZ, is the best choice for hybrid XSAPT-type methods. Much of the present work has therefore been dedicated to finding basis sets that afford converged results for all four energy components. A general trend across all of the energy components is that diffuse functions are important, even in systems where the monomers are charge neutral. This is an important observation given that (in our experience) many computational chemists are hesitant to include diffuse functions, presumably for reasons of cost. Data presented herein make it clear that this omission has deleterious consequences for accuracy. Notably, this is true for the perturbative components of XSAPT (E_{elstv} , E_{exch} , and E_{ind}) that have identical forms in SAPT0; hence, our results underscore the need for diffuse functions in conventional SAPT calculations as well.

As compared to electrostatics or dispersion, the exchange and induction energies are more sensitive to the choice of basis set, and these are not converged unless triple- ζ basis sets are used. Dunning’s correlation-consistent basis sets can certainly be used for this purpose and provide smooth convergence to the CBS limit. However, these basis sets are more expensive than other alternatives that afford similar accuracy. Karlsruhe “def2” basis sets work well in this capacity, although we find that Pople basis sets with additional polarization functions, such as 6-311+G(3df,2pd), can also provide high-quality results, comparable to def2-TZVPD in many cases. The use of Pople basis sets is sometimes maligned in modern electronic structure theory, but they are very efficient in certain quantum chemistry codes that can take advantage of *sp* shells. As applied to $\text{Cl}^-(\text{H}_2\text{O})_{28}$, for example (with Cl^- as one monomer and the water cluster as the other), XSAPT calculations with 6-311+G(3df,2pd) afford a 2 \times speedup over def2-TZVPD despite the fact that the Pople basis set has 253 more functions! The 6-311+G(2df,2p) basis set affords a 5 \times speedup over def2-TZVPD, and interaction energies obtained with either of these Pople basis sets are within 0.5 kcal/mol of the def2-TZVPD value.

Further speedups can be obtained by exploiting separability of the SAPT energy decomposition to evaluate different energy components at different levels of theory. A preliminary version of this idea (which is trivial to implement) is to use a smaller basis set to evaluate δE_{HF} , the correction for induction effects beyond second-order perturbation theory. We find that a minimally augmented double- ζ basis, such as 6-31+G(d) or def2-ma-SVP (the latter of which is introduced as part of the present work), is sufficient to compute δE_{HF} , which is defined by the energy difference and thus converges rapidly. For quadruple- ζ calculations, this mixed-basis procedure affords speedups of 3–4 \times .

For dimers of charge-neutral complexes, there is little reason to push XSAPT to quadruple- ζ basis sets, and we find that a good catch-all basis set is def2-TZVPD, although 6-311++G(3df,2pd) also works very well for charge-neutral monomers. (The Pople basis set exhibits much larger errors for systems containing ions.) For ionic systems, where induction effects are very large, the best results are obtained using def2-ma-QZVP for anions and def2-QZVPD for cations, although def2-TZVPPD affords MAEs that are only about 0.4 kcal/mol larger.

The conclusions outlined above are drawn from tests on small dimers where it is possible to use basis sets of quadruple- ζ quality. Tests on two larger systems, namely, a DNA intercalation complex with 157 atoms and the coronene dimer, (C₂₄H₁₂)₂, appear to indicate that def2-TZVPD and jun-cc-pVTZ results are essentially converged. Whereas for small dimers the XSAPT + MBD method exhibits an accuracy of ~ 1 kcal/mol with respect to CCSD(T)/CBS benchmarks, in these larger systems XSAPT + MBD overestimates the CCSD(T)/CBS benchmark by ≈ 2 kcal/mol but only if the δE_{HF} correction is omitted. The CCSD(T)/CBS benchmark is itself somewhat more strongly bound than alternative QMC benchmarks. The value of δE_{HF} is 2–3 kcal/mol for these large supramolecular complexes, but its inclusion actually degrades the agreement with the benchmarks, for reasons that are unclear but which are also observed, on a smaller scale, in the non-hydrogen-bonded S66 dimers. Given that individual XSAPT + MBD energy components for the S22 dimers are in good agreement with SAPT2+(3)/aug-cc-pVTZ benchmarks, the origin of these discrepancies for larger systems remains an open question that warrants further examination.

■ ASSOCIATED CONTENT

SI Supporting Information

The Supporting Information is available free of charge at <https://pubs.acs.org/doi/10.1021/acs.jctc.1c01302>.

Additional data tables and figures including range-separation parameters, XSAPT + MBD error statistics, SAPT0(KS) + MBD results, and XSAPT + MBD energy components (PDF)

Complete specification of the def2-ma and def2-ha sequence of basis sets (ZIP)

■ AUTHOR INFORMATION

Corresponding Author

John M. Herbert – Department of Chemistry and Biochemistry, The Ohio State University, Columbus, Ohio 43210, United States; orcid.org/0000-0002-1663-2278; Email: herbert@chemistry.ohio-state.edu

Author

Montgomery Gray – Department of Chemistry and Biochemistry, The Ohio State University, Columbus, Ohio 43210, United States

Complete contact information is available at: <https://pubs.acs.org/doi/10.1021/acs.jctc.1c01302>

Notes

The authors declare the following competing financial interest(s): J.M.H. serves on the board of directors of Q-Chem Inc.

■ ACKNOWLEDGMENTS

This work was supported by the U.S. Department of Energy, Office of Basic Energy Sciences, Division of Chemical Sciences, Geosciences, and Biosciences under Award No. DE-SC0008550. Calculations were performed at the Ohio Supercomputer Center.¹¹⁶

■ REFERENCES

- (1) Szalewicz, K. Determination of structure and properties of molecular crystals from first principles. *Acc. Chem. Res.* **2014**, *47*, 3266–3274.
- (2) Brandenburg, J. G.; Grimme, S. Dispersion corrected Hartree-Fock and density functional theory for organic crystal structure prediction. In *Prediction and Calculation of Crystal Structures*; Atahan-Evrenk, Ş., Aspuru-Guzik, A., Eds.; Springer: Heidelberg, 2014; Vol. 345.
- (3) Beran, G. J. O. Modeling polymorphic molecular crystals with electronic structure theory. *Chem. Rev.* **2016**, *116*, 5567–5613.
- (4) Beran, G. J. O.; Heit, Y. N.; Hartman, J. D. Noncovalent interactions in molecular crystals. In *Non-Covalent Interactions in Quantum Chemistry and Physics*; de la Roza, A. O., DiLabio, G. A., Eds.; Elsevier: Amsterdam, 2017; Chapter 10, pp 303–331.
- (5) Price, S. L.; Brandenburg, J. G. Molecular crystal structure prediction. In *Non-Covalent Interactions in Quantum Chemistry and Physics*; de la Roza, A. O., DiLabio, G. A., Eds.; Elsevier: Amsterdam, 2017; Chapter 11, pp 333–363.
- (6) Plevin, M.; Bryce, D. L.; Boisbouvier, J. Direct detection of CH/ π interactions in proteins. *Nat. Chem.* **2010**, *2*, 466–471.
- (7) McGaughey, G. B.; Gagné, M.; Rappé, A. K. π -stacking interactions: Alive and well in proteins. *J. Biol. Chem.* **1998**, *273*, 15458–15463.
- (8) Brandl, M.; Weiss, M. S.; Jabs, A.; Sühnel, J.; Hilgenfeld, R. C-H $\cdots\pi$ interactions in proteins. *J. Mol. Biol.* **2001**, *307*, 357–377.
- (9) He, X.; Fusti-Molnar, L.; Cui, G.; Merz, K. M., Jr. The importance of dispersion and electron correlation in ab initio protein folding. *J. Phys. Chem. B* **2009**, *113*, 5290–5300.
- (10) Xu, Z.; Zhang, Q.; Shi, J.; Zhu, W. Underestimated noncovalent interactions in protein data bank. *J. Chem. Inf. Model.* **2019**, *59*, 3389–3399.
- (11) Parrish, R. M.; Sitkoff, D. F.; Cheney, D. L.; Sherrill, C. D. The surprising importance of peptide bond contacts in drug–protein interactions. *Chem.-Eur. J.* **2017**, *23*, 7887–7890.
- (12) Kumar, K.; Woo, S. M.; Siu, T.; Cortopassi, W. A.; Duarte, F.; Paton, R. S. Cation– π interactions in protein–ligand binding: Theory and data-mining reveal different roles for lysine and arginine. *Chem. Sci.* **2018**, *9*, 2655–2665.
- (13) Sylvestry, N. Toward simple, predictive understanding of protein–ligand interactions: Electronic structure calculations on Torpedo Californica Acetylcholinesterase join forces with the chemist's intuition. *Sci. Rep.* **2020**, *10*, 9219.
- (14) Schriber, J. B.; Nascimento, D. R.; Koutsoukas, A.; Spronk, S. A.; Cheney, D. L.; Sherrill, C. D. CLIFF: A component-based, machine-learned, intermolecular force field. *J. Chem. Phys.* **2021**, *154*, 184110.
- (15) Tkatchenko, A. Current understanding of van der Waals effects in realistic materials. *Adv. Funct. Mater.* **2015**, *25*, 2054–2061.
- (16) Ravva, M. K.; Risko, C.; Brédas, J.-L. Noncovalent interactions in organic electronic materials. In *Non-Covalent Interactions in Quantum Chemistry and Physics*; de la Roza, A. O., DiLabio, G. A., Eds.; Elsevier: Amsterdam, 2017; Chapter 9, pp 277–302.
- (17) Cooper, V. R.; Lam, C. N.; Wang, Y.; Sumpter, B. G. Noncovalent interactions in nanotechnology. In *Non-Covalent Interactions in Quantum Chemistry and Physics*; de la Roza, A. O., DiLabio, G. A., Eds.; Elsevier: Amsterdam, 2017; Chapter 14, pp 417–451.
- (18) Wagner, J. P.; Schreiner, P. R. London dispersion in molecular chemistry—Reconsidering steric effects. *Angew. Chem., Int. Ed. Engl.* **2015**, *54*, 12274–12279.

- (19) Herbert, J. M. Neat, simple, and wrong: Debunking electrostatic fallacies regarding noncovalent interactions. *J. Phys. Chem. A* **2021**, *125*, 7125–7137.
- (20) Carter-Fenk, K.; Lao, K. U.; Herbert, J. M. Predicting and understanding non-covalent interactions using novel forms of symmetry-adapted perturbation theory. *Acc. Chem. Res.* **2021**, *54*, 3679–3690.
- (21) Szalewicz, K.; Patkowski, K.; Jeziorski, B. Intermolecular interactions via perturbation theory: From diatoms to biomolecules. In *Intermolecular Forces and Clusters II*; Wales, D. J., Ed.; Springer-Verlag: Berlin, 2005; Vol. 116.
- (22) Hohenstein, E. G.; Sherrill, C. D. Wavefunction methods for noncovalent interactions. *WIREs Comput. Mol. Sci.* **2012**, *2*, 304–326.
- (23) Szalewicz, K. Symmetry-adapted perturbation theory of intermolecular forces. *WIREs Comput. Mol. Sci.* **2012**, *2*, 254–272.
- (24) Jansen, G. Symmetry-adapted perturbation theory based on density functional theory for noncovalent interactions. *WIREs Comput. Mol. Sci.* **2014**, *4*, 127–144.
- (25) Parker, T. M.; Burns, L. A.; Parrish, R. M.; Ryno, A. G.; Sherrill, C. D. Levels of symmetry adapted perturbation theory (SAPT). I. Efficiency and performance for interaction energies. *J. Chem. Phys.* **2014**, *140*, 094106.
- (26) Patkowski, K. Recent developments in symmetry-adapted perturbation theory. *WIREs Comput. Mol. Sci.* **2020**, *10*, No. e1452.
- (27) Stone, A. J. Physical basis of intermolecular interactions. In *Non-Covalent Interactions in Quantum Chemistry and Physics*; de la Roza, A. O., DiLabio, G. A., Eds.; Elsevier: Amsterdam, 2017; Chapter 1, pp 3–26.
- (28) Francisco, E.; Pendás, A. M. Energy partition analyses: Symmetry-adapted perturbation theory and other techniques. In *Non-Covalent Interactions in Quantum Chemistry and Physics*; de la Roza, A. O., DiLabio, G. A., Eds.; Elsevier: Amsterdam, 2017; Chapter 2, pp 27–64.
- (29) Misquitta, A. Intermolecular interactions. In *Handbook of Computational Chemistry*, 2nd ed.; Leszczynski, J., Kaczmarek-Kedziera, A., Puzyn, T., Papadopoulos, M. G., Reis, H., Shukla, M. K., Eds.; Springer International Publishing: Switzerland, 2017; Chapter 8, pp 295–335.
- (30) Hohenstein, E. G.; Duan, J.; Sherrill, D. C. Origin of the surprising enhancement of electrostatic energies by electron-donating substituents in substituted sandwich benzene dimers. *J. Am. Chem. Soc.* **2011**, *133*, 13244–13247.
- (31) Sherrill, C. D. Energy component analysis of π interactions. *Acc. Chem. Res.* **2013**, *46*, 1020–1028.
- (32) Parrish, R. M.; Sherrill, C. D. Quantum-mechanical evaluation of the π - π versus substituent- π interactions in π stacking: Direct evidence for the Wheeler–Houk picture. *J. Am. Chem. Soc.* **2014**, *136*, 17386–17389.
- (33) Parrish, R. M.; Parker, T. M.; Sherrill, C. D. Chemical assignment of symmetry-adapted perturbation theory interaction energy components: The functional-group SAPT partition. *J. Chem. Theory Comput.* **2014**, *10*, 4417–4431.
- (34) Carter-Fenk, K.; Herbert, J. M. Electrostatics does not dictate the slip-stacked arrangement of aromatic π - π interactions. *Chem. Sci.* **2020**, *11*, 6758–6765.
- (35) Carter-Fenk, K.; Herbert, J. M. Reinterpreting π -stacking. *Phys. Chem. Chem. Phys.* **2020**, *22*, 24870–24886.
- (36) Herbert, J. M.; Carter-Fenk, K. Electrostatics, charge transfer, and the nature of the halide–water hydrogen bond. *J. Phys. Chem. A* **2021**, *125*, 1243–1256.
- (37) Shahbaz, M.; Szalewicz, K. Do semilocal density-functional approximations recover dispersion energies at small intermonomer separations? *Phys. Rev. Lett.* **2018**, *121*, 113402.
- (38) Shahbaz, M.; Szalewicz, K. Evaluation of methods for obtaining dispersion energies used in density functional calculations of intermolecular interactions. *Theor. Chem. Acc.* **2019**, *138*, 25.
- (39) Price, A. J. A.; Bryenton, K. R.; Johnson, E. R. Requirements for an accurate dispersion-corrected density functional. *J. Chem. Phys.* **2021**, *154*, 230902.
- (40) Schmidt, J. R.; Yu, K.; McDaniel, J. G. Transferable next-generation force fields from simple liquids to complex materials. *Acc. Chem. Res.* **2015**, *48*, 548–556.
- (41) Metz, M. P.; Szalewicz, K. Automatic generation of flexible-monomer intermolecular potential energy surfaces. *J. Chem. Theory Comput.* **2020**, *16*, 2317–2339.
- (42) Gray, M.; Herbert, J. M. Simplified tuning of long-range corrected density functionals for symmetry-adapted perturbation theory. *J. Chem. Phys.* **2021**, *155*, 034103.
- (43) Lao, K. U.; Herbert, J. M. Symmetry-adapted perturbation theory with Kohn–Sham orbitals using non-empirically tuned, long-range-corrected density functionals. *J. Chem. Phys.* **2014**, *140*, 044108.
- (44) Hapka, M.; Rajchel, L.; Modrzejewski, M.; Chałasiński, G.; Szczeniński, M. M. Tuned range-separated hybrid functionals in the symmetry-adapted perturbation theory. *J. Chem. Phys.* **2014**, *141*, 134120.
- (45) Szabo, A.; Ostlund, N. S. The correlation energy in the random phase approximation: Intermolecular forces between closed-shell systems. *J. Chem. Phys.* **1977**, *67*, 4351–4360.
- (46) Heßelmann, A. Improved supermolecular second order Møller–Plesset intermolecular interaction energies using time-dependent density functional response theory. *J. Chem. Phys.* **2008**, *128*, 144112.
- (47) Rezáč, J.; Greenwell, C.; Beran, G. J. O. Accurate noncovalent interactions via dispersion-corrected second-order Møller–Plesset perturbation theory. *J. Chem. Theory Comput.* **2018**, *14*, 4711–4721.
- (48) Lao, K. U.; Herbert, J. M. Atomic orbital implementation of extended symmetry-adapted perturbation theory (XSAPT) and benchmark calculations for large supramolecular complexes. *J. Chem. Theory Comput.* **2018**, *14*, 2955–2978.
- (49) Nguyen, B.; Chen, G. P.; Agee, M. M.; Burow, A. M.; Tang, M.; Furché, F. Divergence of many-body perturbation theory for noncovalent interactions of large molecules. *J. Chem. Theory Comput.* **2020**, *16*, 2258–2273.
- (50) Heßelmann, A.; Jansen, G.; Schütz, M. Density-functional theory symmetry-adapted intermolecular perturbation theory with density fitting: A new efficient method to study intermolecular interaction energies. *J. Chem. Phys.* **2005**, *122*, 014103.
- (51) Bukowski, R.; Podaszwa, R.; Szalewicz, K. Efficient calculation of coupled Kohn–Sham dynamic susceptibility functions and dispersion energies with density fitting. *Chem. Phys. Lett.* **2005**, *414*, 111–116.
- (52) Rezáč, J.; Hobza, P. Extrapolation and scaling of the DFT–SAPT interaction energies toward the basis set limit. *J. Chem. Theory Comput.* **2011**, *7*, 685–689.
- (53) Przybytek, M. Dispersion energy of symmetry-adapted perturbation theory from the explicitly correlated F12 approach. *J. Chem. Theory Comput.* **2018**, *14*, 5105–5117.
- (54) Kodrycka, M.; Holzer, C.; Klopper, W.; Patkowski, K. Explicitly correlated dispersion and exchange dispersion energies in symmetry-adapted perturbation theory. *J. Chem. Theory Comput.* **2019**, *15*, 5965–5986; Erratum. *J. Chem. Theory Comput.* **2020**, *16*, 7220–7223.
- (55) Kodrycka, M.; Patkowski, K. Efficient density-fitted explicitly correlated dispersion and exchange dispersion energies. *J. Chem. Theory Comput.* **2021**, *17*, 1435–1456.
- (56) Lao, K. U.; Herbert, J. M. Accurate intermolecular interactions at dramatically reduced cost: XPol+SAPT with empirical dispersion. *J. Phys. Chem. Lett.* **2012**, *3*, 3241–3248.
- (57) Lao, K. U.; Herbert, J. M. An improved treatment of empirical dispersion and a many-body energy decomposition scheme for the explicit polarization plus symmetry-adapted perturbation theory (XSAPT) method. *J. Chem. Phys.* **2013**, *139*, 034107; Erratum. *J. Chem. Phys.* **2014**, *140*, 119901.
- (58) Lao, K. U.; Herbert, J. M. Accurate and efficient quantum chemistry calculations of noncovalent interactions in many-body systems: The XSAPT family of methods. *J. Phys. Chem. A* **2015**, *119*, 235–253.
- (59) Carter-Fenk, K.; Lao, K. U.; Liu, K.-Y.; Herbert, J. M. Accurate and efficient *ab initio* calculations for supramolecular complexes:

- Symmetry-adapted perturbation theory with many-body dispersion. *J. Phys. Chem. Lett.* **2019**, *10*, 2706–2714.
- (60) Liu, K.-Y.; Carter-Fenk, K.; Herbert, J. M. Self-consistent charge embedding at very low cost, with application to symmetry-adapted perturbation theory. *J. Chem. Phys.* **2019**, *151*, 031102.
- (61) Jacobson, L. D.; Herbert, J. M. An efficient, fragment-based electronic structure method for molecular systems: Self-consistent polarization with perturbative two-body exchange and dispersion. *J. Chem. Phys.* **2011**, *134*, 094118.
- (62) Herbert, J. M.; Jacobson, L. D.; Un Lao, K.; Rohrdanz, M. A. Rapid computation of intermolecular interactions in molecular and ionic clusters: Self-consistent polarization plus symmetry-adapted perturbation theory. *Phys. Chem. Chem. Phys.* **2012**, *14*, 7679–7699.
- (63) Jacobson, L. D.; Richard, R. M.; Lao, K. U.; Herbert, J. M. Efficient monomer-based quantum chemistry methods for molecular and ionic clusters. *Annu. Rep. Comput. Chem.* **2013**, *9*, 25–58.
- (64) Herbert, J. M.; Paul, S. K. Interaction energy analysis of monovalent inorganic anions in bulk water versus air/water interface. *Molecules* **2021**, *26*, 6719.
- (65) Moszyński, R.; Cybulski, S. M.; Chałasiński, G. Many-body theory of intermolecular induction interactions. *J. Chem. Phys.* **1994**, *100*, 4998–5010.
- (66) Iikura, H.; Tsuneda, T.; Yanai, T.; Hirao, K. A long-range correction scheme for generalized-gradient-approximation exchange functionals. *J. Chem. Phys.* **2001**, *115*, 3540–3544.
- (67) Rohrdanz, M. A.; Herbert, J. M. Simultaneous benchmarking of ground- and excited-state properties with long-range-corrected density functional theory. *J. Chem. Phys.* **2008**, *129*, 034107.
- (68) Rohrdanz, M. A.; Martins, K. M.; Herbert, J. M. A long-range-corrected density functional that performs well for both ground-state properties and time-dependent density functional theory excitation energies, including charge-transfer excited states. *J. Chem. Phys.* **2009**, *130*, 054112.
- (69) Alam, B.; Morrison, A. F.; Herbert, J. M. Charge separation and charge transfer in the low-lying excited states of pentacene. *J. Phys. Chem. C* **2020**, *124*, 24653–24666.
- (70) Modrzejewski, M.; Rajchel, Ł.; Chalasinski, G.; Szczesniak, M. M. Density-dependent onset of the long-range exchange: A key to donor–acceptor properties. *J. Phys. Chem. A* **2013**, *117*, 11580–11586.
- (71) Gao, J.; Truhlar, D. G.; Wang, Y.; Mazack, M. J. M.; Löffler, P.; Provorse, M. R.; Rehak, P. Explicit polarization: A quantum mechanical framework for developing next generation force fields. *Acc. Chem. Res.* **2014**, *47*, 2837–2845.
- (72) Marenich, A. V.; Jerome, S. V.; Cramer, C. J.; Truhlar, D. G. Charge model 5: An extension of Hirshfeld population analysis for the accurate description of molecular interactions in gaseous and condensed phases. *J. Chem. Theory Comput.* **2012**, *8*, 527–541.
- (73) Ambrosetti, A.; Reilly, A. M.; DiStasio, R. A., Jr.; Tkatchenko, A. Long-range correlation energy calculated from coupled atomic response functions. *J. Chem. Phys.* **2014**, *140*, 18A508.
- (74) Hermann, J.; DiStasio, R. A., Jr.; Tkatchenko, A. First-principles models for van der Waals interactions in molecules and materials: Concepts, theory, and applications. *Chem. Rev.* **2017**, *117*, 4714–4758.
- (75) Epifanovsky, E.; Gilbert, A. T. B.; Feng, X.; Lee, J.; Mao, Y.; Mardirossian, N.; Pokhilko, P.; White, A. F.; Coons, M. P.; Dempwolff, A. L.; Gan, Z.; Hait, D.; Horn, P. R.; Jacobson, L. D.; Kaliman, I.; Kussmann, J.; Lange, A. W.; Lao, K. U.; Levine, D. S.; Liu, J.; McKenzie, S. C.; Morrison, A. F.; Nanda, K. D.; Plasser, F.; Rehn, D. R.; Vidal, M. L.; You, Z.-Q.; Zhu, Y.; Alam, B.; Albrecht, B. J.; Aldossary, A.; Alguire, E.; Andersen, J. H.; Athavale, V.; Barton, D.; Begam, K.; Behn, A.; Bellonzi, N.; Bernard, Y. A.; Berquist, E. J.; Burton, H. G. A.; Carreras, A.; Carter-Fenk, K.; Chakraborty, R.; Chien, A. D.; Closser, K. D.; Cofer-Shabica, V.; Dasgupta, S.; de Wergifosse, M.; Deng, J.; Diedenhofen, M.; Do, H.; Ehlert, S.; Fang, P.-T.; Fatehi, S.; Feng, Q.; Friedhoff, T.; Gayvert, J.; Ge, Q.; Gidofalvi, G.; Goldey, M.; Gomes, J.; Gonzalez-Espinoza, C. E.; Gulania, S.; Gunina, A. O.; Hanson-Heine, M. W. D.; Harbach, P. H. P.; Hauser, A.; Herbst, M. F.; Hernandez Vera, M.; Hodecker, M.; Holden, Z. C.; Houck, S.; Huang, X.; Hui, K.; Huynh, B. C.; Ivanov, M.; Jasz, A.; Ji, H.; Jiang, H.; Kaduk, B.; Kahler, S.; Khistyayev, K.; Kim, J.; Kis, G.; Klunzinger, P.; Koczor-Benda, Z.; Koh, J. H.; Kosenkov, D.; Koulalias, L.; Kowalczyk, T.; Krauter, C. M.; Kue, K.; Kunitsa, A.; Kus, T.; Ladjanski, I.; Landau, A.; Lawler, K. V.; Lefrancois, D.; Lehtola, S.; Li, R. R.; Li, Y.-P.; Liang, J.; Liebenthal, M.; Lin, H.-H.; Lin, Y.-S.; Liu, F.; Liu, K.-Y.; Loipersberger, M.; Luenser, A.; Manjanath, A.; Manohar, P.; Mansoor, E.; Manzer, S. F.; Mao, S.-P.; Marenich, A. V.; Markovich, T.; Mason, S.; Maurer, S. A.; McLaughlin, P. F.; Menger, M. F. S. J.; Mewes, J.-M.; Mewes, S. A.; Morgante, P.; Mullinax, J. W.; Oosterbaan, K. J.; Paran, G.; Paul, A. C.; Paul, S. K.; Pavosevic, F.; Pei, Z.; Prager, S.; Proynov, E. I.; Rak, A.; Ramos-Cordoba, E.; Rana, B.; Rask, A. E.; Rettig, A.; Richard, R. M.; Rob, F.; Rossomme, E.; Scheele, T.; Scheurer, M.; Schneider, M.; Sergueev, N.; Sharada, S. M.; Skomorowski, W.; Small, D. W.; Stein, C. J.; Su, Y.-C.; Sundstrom, E. J.; Tao, Z.; Thirman, J.; Tornai, G. J.; Tsuchimochi, T.; Tubman, N. M.; Veccham, S. P.; Vydrov, O.; Wenzel, J.; Witte, J.; Yamada, A.; Yao, K.; Yeganeh, S.; Yost, S. R.; Zech, A.; Zhang, I. Y.; Zhang, X.; Zhang, Y.; Zuev, D.; Aspuru-Guzik, A.; Bell, A. T.; Besley, N. A.; Bravaya, K. B.; Brooks, B. R.; Casanova, D.; Chai, J.-D.; Coriani, S.; Cramer, C. J.; Cserey, G.; DePrince, A. E.; DiStasio, R. A.; Dreuw, A.; Dunietz, B. D.; Furlani, T. R.; Goddard, W. A.; Hammes-Schiffer, S.; Head-Gordon, T.; Hehre, W. J.; Hsu, C.-P.; Jagau, T.-C.; Jung, Y.; Klamt, A.; Kong, J.; Lambrecht, D. S.; Liang, W.; Mayhall, N. J.; McCurdy, C. W.; Neaton, J. B.; Ochsenfeld, C.; Parkhill, J. A.; Peverati, R.; Rassolov, V. A.; Shao, Y.; Slipchenko, L. V.; Stauch, T.; Steele, R. P.; Subotnik, J. E.; Thom, A. J. W.; Tkatchenko, A.; Truhlar, D. G.; Van Voorhis, T.; Wesolowski, T. A.; Whaley, K. B.; Woodcock, H. L.; Zimmerman, P. M.; Faraji, S.; Gill, P. M. W.; Head-Gordon, M.; Herbert, J. M.; Krylov, A. I. Software for the frontiers of quantum chemistry: An overview of developments in the Q-Chem 5 package. *J. Chem. Phys.* **2021**, *155*, 084801.
- (76) Williams, H. L.; Mas, E. M.; Szalewicz, K.; Jeziorski, B. On the effectiveness of monomer-, dimer-, and bond-centered basis functions in calculations of intermolecular interaction energies. *J. Chem. Phys.* **1995**, *103*, 7374–7391.
- (77) Carter-Fenk, K.; Mundy, C. J.; Herbert, J. M. Natural charge-transfer analysis: Eliminating spurious charge-transfer states in time-dependent density functional theory via diabaticization, with application to projection-based embedding. *J. Chem. Theory Comput.* **2021**, *17*, 4195–4210.
- (78) Gill, P. M. W.; Johnson, B. G.; Pople, J. A. A standard grid for density-functional calculations. *Chem. Phys. Lett.* **1993**, *209*, 506–512.
- (79) Frisch, M. J.; Pople, J. A.; Binkley, J. S. Self-consistent molecular orbital methods 25. Supplementary functions for Gaussian basis sets. *J. Chem. Phys.* **1984**, *80*, 3265–3269.
- (80) Weigend, F.; Ahlrichs, R. Balanced basis sets of split valence, triple zeta valence and quadruple zeta valence quality for H to Rn: Design and assessment of accuracy. *Phys. Chem. Chem. Phys.* **2005**, *7*, 3297–3305.
- (81) Rappoport, D.; Furche, F. Property-optimized Gaussian basis sets for molecular response calculations. *J. Chem. Phys.* **2010**, *133*, 134105.
- (82) Dunning, T. H., Jr. Gaussian basis sets for use in correlated molecular calculations. I. The atoms boron through neon and hydrogen. *J. Chem. Phys.* **1989**, *90*, 1007–1023.
- (83) Kendall, R. A.; Dunning, T. H., Jr.; Harrison, R. J. Electron affinities of the first-row atoms revisited. Systematic basis sets and wave functions. *J. Chem. Phys.* **1992**, *96*, 6796–6806.
- (84) Papajak, E.; Zheng, J.; Xu, X.; Leverentz, H. R.; Truhlar, D. G. Perspectives on basis sets beautiful: Seasonal plantings of diffuse basis functions. *J. Chem. Theory Comput.* **2011**, *7*, 3027–3034.
- (85) Zheng, J.; Xu, X.; Truhlar, D. G. Minimally augmented Karlsruhe basis sets. *Theor. Chem. Acc.* **2011**, *128*, 295–305.
- (86) Rezáč, J.; Riley, K. E.; Hobza, P. S66: A well-balanced database of benchmark interaction energies relevant to biomolecular structures. *J. Chem. Theory Comput.* **2011**, *7*, 2427–2438; Erratum. *J. Chem. Theory Comput.* **2014**, *10*, 1359–1360.

- (87) Lao, K. U.; Schäffer, R.; Jansen, G.; Herbert, J. M. Accurate description of intermolecular interactions involving ions using symmetry-adapted perturbation theory. *J. Chem. Theory Comput.* **2015**, *11*, 2473–2486.
- (88) Zahn, S.; MacFarlane, D. R.; Izgorodina, E. I. Assessment of Kohn–Sham density functional theory and Møller–Plesset perturbation theory for ionic liquids. *Phys. Chem. Chem. Phys.* **2013**, *15*, 13664–13675.
- (89) Löwdin, P.-O. Twenty-five years of Sanibel symposia: A brief historic and scientific survey. *Int. J. Quantum Chem. Symp.* **1985**, *28*, 19–37.
- (90) Sedlak, R.; Janowski, T.; Pitoňák, M.; Řezáč, J.; Pulay, P.; Hobza, P. Accuracy of quantum chemical methods for large noncovalent complexes. *J. Chem. Theory Comput.* **2013**, *9*, 3364–3374.
- (91) Řezáč, J.; Hobza, P. Describing noncovalent interactions beyond the common approximations: How accurate is the “gold standard”, CCSD(T) at the complete basis set limit? *J. Chem. Theory Comput.* **2013**, *9*, 2151–2155.
- (92) Jurečka, P.; Šponer, J.; Černý, J.; Hobza, P. Benchmark database of accurate (MP2 and CCSD(T) complete basis set limit) interaction energies of small model complexes, DNA base pairs, and amino acid pairs. *Phys. Chem. Chem. Phys.* **2006**, *8*, 1985–1993.
- (93) Flick, J. C.; Kosenkov, D.; Hohenstein, E. G.; Sherrill, C. D.; Slipchenko, L. V. Accurate prediction of noncovalent interaction energies with the effective fragment potential method: Comparison of energy components to symmetry-adapted perturbation theory for the S22 test set. *J. Chem. Theory Comput.* **2012**, *8*, 2835–2843; Erratum. *J. Chem. Theory Comput.* **2014**, *10*, 4759–4760.
- (94) Bultinck, P.; Ayers, P. W.; Fias, S.; Tiels, K.; Van Alsenoy, C. Uniqueness and basis set dependence of iterative Hirshfeld charges. *Chem. Phys. Lett.* **2007**, *444*, 205–208.
- (95) Bultinck, P.; Van Alsenoy, C.; Ayers, P. W.; Carbó-Dorca, R. Critical analysis and extension of the Hirshfeld atoms in molecules. *J. Chem. Phys.* **2007**, *126*, 144111.
- (96) Bultinck, P.; Cooper, D. L.; Van Neck, D. Comparison of the Hirshfeld-I and iterated stockholder atoms in molecules schemes. *Phys. Chem. Chem. Phys.* **2009**, *11*, 3424–3429.
- (97) Bučko, T.; Lebègue, S.; Hafner, J.; Ángyán, J. G. Improved density dependent correction for the description of London dispersion forces. *J. Chem. Theory Comput.* **2013**, *9*, 4293–4299.
- (98) Bučko, T.; Lebègue, S.; Ángyán, J. G.; Hafner, J. Extending the applicability of the Tkatchenko–Scheffler dispersion correction via iterative Hirshfeld partitioning. *J. Chem. Phys.* **2014**, *141*, 034114.
- (99) Gould, T.; Lebègue, S.; Ángyán, J. G.; Bučko, T. A fractionally ionic approach to polarizability and van der Waals many-body dispersion calculations. *J. Chem. Theory Comput.* **2016**, *12*, 5920–5930.
- (100) Hermann, J.; Tkatchenko, A. Density functional model for van der Waals interactions: Unifying many-body atomic approaches with nonlocal functionals. *Phys. Rev. Lett.* **2020**, *124*, 146401.
- (101) Paul, S. K.; Herbert, J. M. Probing interfacial effects on ionization energies: The surprising banality of anion–water hydrogen bonding at the air/water interface. *J. Am. Chem. Soc.* **2021**, *143*, 10189–10202.
- (102) Lao, K. U.; Herbert, J. M. A simple correction for nonadditive dispersion within extended symmetry-adapted perturbation theory (XSAPT). *J. Chem. Theory Comput.* **2018**, *14*, 5128–5142.
- (103) Shannon, R. D. Revised effective ionic radii and systematic studies of interatomic distances in halides and chalcogenides. *Acta Cryst. A* **1976**, *32*, 751–767.
- (104) Marshall, M. S.; Burns, L. A.; Sherrill, C. D. Basis set convergence of the coupled-cluster correction, $\delta_{\text{MP2}}^{\text{CCSD(T)}}$: Best practices for benchmarking non-covalent interactions and the attendant revision of the S22, NBC10, and HSG databases. *J. Chem. Phys.* **2011**, *135*, 194102.
- (105) Stiborova, M.; Sejbal, J.; Borek-Dohalska, L.; Aimova, D.; Poljakova, J.; Forsterova, K.; Rupertova, M.; Wiesner, J.; Hudecek, J.; Wiessler, M.; Frei, E. The anticancer drug ellipticine forms covalent DNA adducts, mediated by human cytochromes P450, through metabolism to 13-hydroxyellipticine and ellipticine N^2 -oxide. *Cancer Res.* **2004**, *64*, 8374–8380.
- (106) DiStasio, R. A., Jr.; von Lilienfeld, O. A.; Tkatchenko, A. Collective many-body van der Waals interactions in molecular systems. *Proc. Natl. Acad. Sci. U.S.A.* **2012**, *109*, 14791–14795.
- (107) Benali, A.; Shulenburger, L.; Romero, N. A.; Kim, J.; von Lilienfeld, O. A. Application of diffusion Monte Carlo to materials dominated by van der Waals interactions. *J. Chem. Theory Comput.* **2014**, *10*, 3417–3422.
- (108) Ballesteros, F.; Dunivan, S.; Lao, K. U. Coupled cluster benchmarks of large noncovalent complexes: The L7 dataset as well as DNA-ellipticine and buckycatcher-fullerene. *J. Chem. Phys.* **2021**, *154*, 154104.
- (109) Al-Hamdani, Y. S.; Nagy, P. R.; Zen, A.; Barton, D.; Kállay, M.; Brandenburg, J. G.; Tkatchenko, A. Interactions between large molecules pose a puzzle for reference quantum mechanical methods. *Nat. Commun.* **2021**, *12*, 3927.
- (110) Benali, A.; Shin, H.; Heinonen, O. Quantum Monte Carlo benchmarking of large noncovalent complexes in the L7 benchmark set. *J. Chem. Phys.* **2020**, *153*, 194113.
- (111) Riplinger, C.; Neese, F. An efficient and near linear scaling pair natural orbital based local coupled cluster method. *J. Chem. Phys.* **2013**, *138*, 034106.
- (112) Riplinger, C.; Sandhoefer, B.; Hansen, A.; Neese, F. Natural triple excitations in local coupled cluster calculations with pair natural orbitals. *J. Chem. Phys.* **2013**, *139*, 134101.
- (113) Sparta, M.; Neese, F. Chemical applications carried out by local pair natural orbital based coupled-cluster methods. *Chem. Soc. Rev.* **2014**, *43*, 5032–5041.
- (114) Sorathia, K.; Tew, D. P. Basis set extrapolation in pair natural orbital theories. *J. Chem. Phys.* **2020**, *153*, 174112.
- (115) Altun, A.; Ghosh, S.; Riplinger, C.; Neese, F.; Bistoni, G. Addressing the system-size dependence of the local approximation error in coupled-cluster calculations. *J. Phys. Chem. A* **2021**, *125*, 9932–9939.
- (116) Ohio Supercomputer Center, <http://osc.edu/ark:/19495/f5s1ph73> (accessed March 4, 2022).